

Flavor Violating Higgs Decays

Roni Harnik,^{1,*} Joachim Kopp,^{1,2,†} and Jure Zupan^{3,‡}

¹*Fermilab, P.O. Box 500, Batavia, IL 60510, USA*

²*Max Planck Institute for Nuclear Physics,*

PO Box 103980, 69029 Heidelberg, Germany

³*Department of Physics, University of Cincinnati, Cincinnati, Ohio 45221, USA*

(Dated: September 10, 2012)

Abstract

We study a class of nonstandard interactions of the newly discovered 125 GeV Higgs-like resonance that are especially interesting probes of new physics: flavor violating Higgs couplings to leptons and quarks. These interaction can arise in many frameworks of new physics at the electroweak scale such as two Higgs doublet models, extra dimensions, or models of compositeness. We rederive constraints on flavor violating Higgs couplings using data on rare decays, electric and magnetic dipole moments, and meson oscillations. We confirm that flavor violating Higgs boson decays to leptons can be sizeable with, e.g., $h \rightarrow \tau\mu$ and $h \rightarrow \tau e$ branching ratios of $\mathcal{O}(10\%)$ perfectly allowed by low energy constraints. We estimate the current LHC limits on $h \rightarrow \tau\mu$ and $h \rightarrow \tau e$ decays by recasting existing searches for the SM Higgs in the $\tau\tau$ channel and find that these bounds are already stronger than those from rare tau decays. We also show that these limits can be improved significantly with dedicated searches and we outline a possible search strategy. Flavor violating Higgs decays therefore present an opportunity for discovery of new physics which in some cases may be easier to access experimentally than flavor conserving deviations from the Standard Model Higgs framework.

*Email: roni@fnal.gov

†Email: jkopp@fnal.gov

‡Email: zupanje@ucmail.uc.edu

I. INTRODUCTION

Both ATLAS and CMS have recently announced the discovery of a Higgs-like resonance with a mass of $m_h \simeq 125$ GeV [1–4], further supported by combined Tevatron data [5]. An interesting question is whether the properties of this resonance are consistent with the Standard Model (SM) Higgs boson. Deviations from the SM predictions could point to the existence of a secondary mechanism of electroweak symmetry breaking or to other types of new physics not too far above the electroweak scale. While there is a large ongoing experimental effort to measure precisely the decay rates into the channels that dominate for the SM Higgs, it is equally important to search for Higgs decays into channels that are subdominant or absent in the SM. For instance, since the couplings of the Higgs boson to quarks of the first two generations and to leptons are suppressed by small Yukawa couplings in the SM, new physics contributions can easily dominate over the SM predictions. Another possibility, and the main topic of this paper, is *flavor violating* (FV) Higgs decays, for instance into $\tau\mu$ or μe final states. The study of FV couplings of the Higgs boson has a long history [6–26]. In this paper, we refine the indirect bounds on the FV couplings. Most importantly, we discuss in detail possible search strategies for FV Higgs decays at the LHC and derive for the first time limits from LHC data.

As pointed out in the previous literature, and confirmed by the present analysis, the indirect constraints on many FV Higgs decays are rather weak. In particular, the branching ratios for $h \rightarrow \tau\mu$ and $h \rightarrow \tau e$ can reach up to 10% [24]. In fact, for $h \rightarrow \tau\mu$ and $h \rightarrow \tau e$ already now¹, without targeted searches, the LHC is placing limits that are comparable to or even stronger than those from rare τ decays. As we shall see later, re-casting a $h \rightarrow \tau\tau$ analysis with 4.7 fb^{-1} of 7 TeV ATLAS data [27] gives a bound on the branching fraction of the Higgs into $\tau\mu$ or τe around 10%. We will also demonstrate that dedicated searches can be much more sensitive.

These decays could thus give a striking signature of new physics at the LHC, and we strongly encourage our experimental colleagues to include them in their searches. Another experimentally interesting set of decay channels are flavor conserving decays to the first two generations, e.g., $h \rightarrow \mu^+\mu^-$, on which we will comment further below. We emphasize that

¹ By $h \rightarrow \tau\mu$ we always mean the sum of $h \rightarrow \tau^+\mu^-$ and $h \rightarrow \tau^-\mu^+$ and similarly for the other decay modes.

large deviations from the SM do not require very exotic flavor structures. A branching ratio for $h \rightarrow \tau\mu$ comparable to the one for $h \rightarrow \tau\tau$, or a $h \rightarrow \mu^+\mu^-$ branching ratio a few times larger than in the SM can arise in many models of flavor (for instance in models with continuous and/or discrete flavor symmetries [28], or in Randall-Sundrum models [29]) as long as there is new physics at the electroweak scale and not just the SM. The lepton flavor violating decay $h \rightarrow \tau\mu$ has been studied in [11], and it was found that the branching ratio for this decay can be up to 10% in certain Two Higgs Doublet Models (2HDMs).

In fact, there may already be experimental hints that the Higgs couplings to fermions may not be SM-like. For instance, the BaBar collaboration recently announced a 3.4σ indication of flavor universality violation in $b \rightarrow c\tau\nu$ transitions [30], which can be explained for instance by an extended Higgs sector with nontrivial flavor structure [31].

The paper is organized as follows. In Sec. II we introduce the theoretical framework we will use to parameterize the flavor violating decays of the Higgs. In Sec. III we derive bounds on flavor violating Higgs couplings to leptons and translate these bounds into limits on the Higgs decay branching fractions to the various flavor violating final states. In Sec. IV we do the same for flavor violating couplings to quarks. We shall see that decays of the Higgs to $\tau\mu$ and to τe with sizeable branching fractions are allowed, and that also flavor violating couplings of the Higgs to top quarks are only weakly constrained. Motivated by this we turn to the LHC in Section V and estimate the current bounds on Higgs decays to $\tau\mu$ and τe using data from an existing $h \rightarrow \tau\tau$ search. We also discuss a strategy for a dedicated $h \rightarrow \tau\mu$ search and comment on differences with the SM $h \rightarrow \tau\tau$ searches. We will see that the LHC can make significant further progress in probing the Higgs' flavor violating parameters space with existing data. We conclude in Section VI. In the appendices, we give more details on the calculation of constraints from low-energy observables.

II. THE FRAMEWORK

After electroweak symmetry breaking (EWSB) the fermionic mass terms and the couplings of the Higgs boson to fermion pairs in the mass basis are in general

$$\mathcal{L}_Y = -m_i \bar{f}_L^i f_R^i - Y_{ij} (\bar{f}_L^i f_R^j) h + h.c. + \dots, \quad (1)$$

where ellipses denote nonrenormalizable couplings involving more than one Higgs field operator. In our notation, $f_L = q_L, \ell_L$ are $SU(2)_L$ doublets, $f_R = u_R, d_R, \nu_R, \ell_R$ the weak singlets, and indices run over generations and fermion flavors (quarks and leptons) with summation implicitly understood. In the SM the Higgs couplings are diagonal, $Y_{ij} = (m_i/v)\delta_{ij}$, but in general NP models the structure of the Y_{ij} can be very different. Note that we use the normalization $v = 246$ GeV here. The goal of the paper is to set bounds on Y_{ij} and identify interesting channels for Higgs decays at the LHC. Throughout we will assume that the Higgs is the only additional degree of freedom with mass $\mathcal{O}(100$ GeV) and that the Y_{ij} 's are the only source of flavor violation. These assumptions are not necessarily valid in general, but will be a good approximation in many important classes of new physics frameworks. Let us now show how $Y_{ij} \neq (m_i/v)\delta_{ij}$ can arise in two qualitatively different categories of NP models.

a. A single Higgs theory. Let us first explore the possibility that the Higgs is the only field that causes EWSB (see also [10, 15, 19, 23, 32–34]). For simplicity let us also assume that at energies below ~ 200 GeV the spectrum consists solely of the SM particles: three generations of quarks and leptons, the SM gauge bosons and the Higgs at 125 GeV. Additional heavy fields (e.g. scalar or fermionic partners which address the hierarchy problem) can be integrated out, so that we can work in effective field theory (EFT)—the effective Standard Model. In addition to the SM Lagrangian

$$\mathcal{L}_{SM} = \bar{f}_L^j i \not{D} f_L^j + \bar{f}_R^j i \not{D} f_R^j - [\lambda_{ij}(\bar{f}_L^i f_R^j)H + h.c.] + D_\mu H^\dagger D^\mu H - \lambda_H \left(H^\dagger H - \frac{v^2}{2} \right)^2, \quad (2)$$

there are then also higher dimensional terms due to the heavy degrees of freedom that were integrated out:

$$\Delta\mathcal{L}_Y = -\frac{\lambda'_{ij}}{\Lambda^2}(\bar{f}_L^i f_R^j)H(H^\dagger H) + h.c. + \dots, \quad (3)$$

Here we have written out explicitly only the terms that modify the Yukawa interactions. We can truncate the expansion after the terms of dimension 6, since these already suffice to completely decouple the values of the fermion masses from the values of fermion couplings to the Higgs boson. Additional dimension 6 operators involving derivatives include

$$\Delta\mathcal{L}_D = \frac{\lambda_L^{ij}}{\Lambda^2}(\bar{f}_L^i \gamma^\mu f_L^j)(H^\dagger i \overleftrightarrow{D}_\mu H) + \frac{\lambda_R^{ij}}{\Lambda^2}(\bar{f}_R^i \gamma^\mu f_R^j)(H^\dagger i \overleftrightarrow{D}_\mu H) + \dots, \quad (4)$$

where $(H^\dagger i \overleftrightarrow{D}_\mu H) \equiv H^\dagger i D_\mu H - (i D_\mu H^\dagger)H$. The couplings λ'_{ij} are complex in general, while the $\lambda_{L,R}^{ij}$ are real. The derivative couplings do not give rise to fermion-fermion-Higgs

couplings after EWSB and are irrelevant for our analysis. In Eq. (4) there are in principle also terms of the form $(\bar{f}_{L,R}^i i \not{D} f_{L,R}^j) H^\dagger H$, which, however, can be shown to be equivalent to (3) by using equations of motion.

After electroweak symmetry breaking (EWSB) and diagonalization of the mass matrices, one obtains the Yukawa Lagrangian in Eq. (1), with

$$\sqrt{2}m = V_L \left[\lambda + \frac{v^2}{2\Lambda^2} \lambda' \right] V_R^\dagger v, \quad \sqrt{2}Y = V_L \left[\lambda + 3 \frac{v^2}{2\Lambda^2} \lambda' \right] V_R^\dagger, \quad (5)$$

where the unitary matrices V_L, V_R are those which diagonalize the mass matrix, and $v = 246$ GeV. In the mass basis we can write

$$Y_{ij} = \frac{m_i}{v} \delta_{ij} + \frac{v^2}{\sqrt{2}\Lambda^2} \hat{\lambda}_{ij}, \quad (6)$$

where $\hat{\lambda} = V_L \lambda' V_R$. In the limit $\Lambda \rightarrow \infty$ one obtains the SM, where the Yukawa matrix Y is diagonal, $Yv = m$. For Λ of the order of the electroweak scale, on the other hand, the mass matrix and the couplings of the Higgs to fermions can be very different as $\hat{\lambda}$ is in principle an arbitrary non-diagonal matrix.

Taking the off diagonal Yukawa couplings nonzero can come with a theoretical price. Consider, for instance, a two flavor mass matrix involving τ and μ . If the off-diagonal entries are very large the mass spectrum is generically not hierarchical. A hierarchical spectrum would require a delicate cancellation among the various terms in Eq. (5). Tuning is avoided if [35]

$$|Y_{\tau\mu} Y_{\mu\tau}| \lesssim \frac{m_\mu m_\tau}{v^2}, \quad (7)$$

with similar conditions for the other off diagonal elements. Even though we will keep this condition in the back of our minds, we will not restrict the parameter space to fulfill it.

b. Models with several sources of EWSB: Let us now discuss the case where the Higgs at 125 GeV is not the only scalar that breaks electroweak symmetry. The modification of the above discussion is straightforward. The additional sources of EWSB are assumed to be heavy and can thus still be integrated out. Their EWSB effects can be described by a spurion χ that formally transforms under electroweak global symmetry and then obtains a vacuum expectation value (vev), which breaks the electroweak symmetry. If χ has the quantum numbers $(2, 1/2)$ under $SU(2)_L \times U(1)_Y$ it can contribute to quark and lepton

masses.² This allows the Yukawa interactions Y of the 125 GeV Higgs to be misaligned with respect to the fermion mass matrix m in Eq. (1).

The simplest example for a full theory of this class is a type III two Higgs doublet model (2HDM) where both Higgses obtain a vev and couple to fermions. In the full theory both of the scalars then have a Lagrangian of the form (1)

$$\mathcal{L}_Y = -m_i \bar{f}_L^i f_R^i - Y_{ij}^a (\bar{f}_L^i f_R^j) h^a + h.c. + \dots, \quad (8)$$

where the index a runs over all the scalars (with Y_{ij}^a imaginary for pseudoscalars), and m_i receives contributions from both vevs. In addition there is also a scalar potential which mixes the two Higgses. Diagonalizing the Higgs mass matrix then also changes Y_{ij}^a , but removes the Higgs mixing. For our purposes it is simplest to work in the Higgs mass basis. All the results for a single Higgs are then trivially modified, replacing our final expressions below by a sum over several Higgses. For a large mass gap, where only one Higgs is light, the contributions from the heavier Higgs are power suppressed, unless its flavor violating Yukawa couplings are parametrically larger than those of the light Higgs. The contributions from the heavy Higgs correspond to the higher dimensional operators discussed in the previous paragraph. This example can be trivially generalized to models with many Higgs doublets.

We next derive constraints on flavor violating Higgs couplings and work out the allowed branching fractions for flavor violation Higgs decays. In placing the bounds we will neglect the FV contributions of the remaining states in the full theory. Our bounds thus apply barring cancellations with these other terms.

III. LEPTONIC FLAVOR VIOLATING HIGGS DECAYS

The FV decays $h \rightarrow e\mu, e\tau, \mu\tau$ arise at tree level from the assumed flavor violating Yukawa interactions, Eq. (1), where the relevant terms are explicitly

$$\mathcal{L}_Y \supset -Y_{e\mu} \bar{e}_L \mu_R h - Y_{\mu e} \bar{\mu}_L e_R h - Y_{e\tau} \bar{e}_L \tau_R h - Y_{\tau e} \bar{\tau}_L e_R h - Y_{\mu\tau} \bar{\mu}_L \tau_R h - Y_{\tau\mu} \bar{\tau}_L \mu_R h + h.c.. \quad (9)$$

² A spurion which transforms as a triplet can also contribute to Majorana masses for neutrinos.

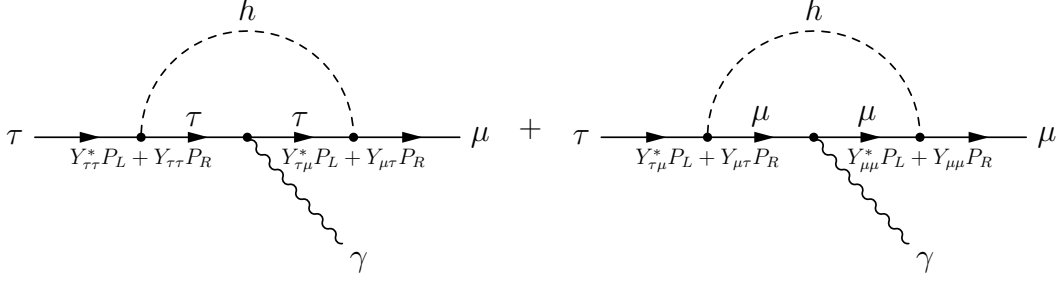


Figure 1: Diagrams contributing to the flavor violating decay $\tau \rightarrow \mu\gamma$, mediated by a Higgs boson with flavor violating Yukawa couplings.

The bounds on the FV Yukawa couplings are collected in Table I, where for simplicity of presentation the flavor diagonal muon and tau Yukawa couplings,

$$\mathcal{L}_Y \supset -Y_{\mu\mu}\bar{\mu}_L\mu_R h - Y_{\tau\tau}\bar{\tau}_L\tau_R h + h.c. , \quad (10)$$

were set equal to their respective SM values $(Y_{\mu\mu})_{\text{SM}} = m_\mu/v$, $(Y_{\tau\tau})_{\text{SM}} = m_\tau/v$. Similar bounds on FV Higgs couplings to quarks are collected in Table II. Similar constraints on flavor violating Higgs decays have been present recently also in [24]. While our results agree qualitatively with previous ones, small numerical differences are expected because we avoid some of the approximations made by previous authors. We also consider some constraining processes not discussed before.

We first give more details on how the bounds in Tables I and II were obtained and then move on to predictions for the allowed sizes of the FV Higgs decays.

A. Constraints from $\tau \rightarrow \mu\gamma$, $\tau \rightarrow e\gamma$ and $\mu \rightarrow e\gamma$

The effective Lagrangian for the $\tau \rightarrow \mu\gamma$ decay is given by

$$\mathcal{L}_{\text{eff}} = c_L Q_{L\gamma} + c_R Q_{R\gamma} + h.c. , \quad (11)$$

where the dim-5 electromagnetic penguin operators are

$$Q_{L\gamma,R\gamma} = \frac{e}{8\pi^2} m_\tau (\bar{\mu} \sigma^{\alpha\beta} P_{L,R} \tau) F_{\alpha\beta} , \quad (12)$$

with α, β the Lorentz indices and $F_{\alpha\beta}$ the electromagnetic field strength tensor. The Wilson coefficients c_L and c_R receive contributions from the two 1-loop diagrams shown in Fig. 1 (with the first one dominant), and a comparable contribution from Barr-Zee type 2-loop

Channel	Coupling	Bound
$\mu \rightarrow e\gamma$	$\sqrt{ Y_{\mu e} ^2 + Y_{e\mu} ^2}$	$< 3.6 \times 10^{-6}$
$\mu \rightarrow 3e$	$\sqrt{ Y_{\mu e} ^2 + Y_{e\mu} ^2}$	$\lesssim 3.1 \times 10^{-5}$
electron $g - 2$	$\text{Re}(Y_{e\mu}Y_{\mu e})$	$-0.019 \dots 0.026$
electron EDM	$ \text{Im}(Y_{e\mu}Y_{\mu e}) $	$< 9.8 \times 10^{-8}$
$\mu \rightarrow e$ conversion	$\sqrt{ Y_{\mu e} ^2 + Y_{e\mu} ^2}$	$< 1.2 \times 10^{-5}$
$M-\bar{M}$ oscillations	$ Y_{\mu e} + Y_{e\mu}^* $	< 0.079
$\tau \rightarrow e\gamma$	$\sqrt{ Y_{\tau e} ^2 + Y_{e\tau} ^2}$	< 0.014
$\tau \rightarrow 3e$	$\sqrt{ Y_{\tau e} ^2 + Y_{e\tau} ^2}$	$\lesssim 0.12$
electron $g - 2$	$\text{Re}(Y_{e\tau}Y_{\tau e})$	$[-2.1 \dots 2.9] \times 10^{-3}$
electron EDM	$ \text{Im}(Y_{e\tau}Y_{\tau e}) $	$< 1.1 \times 10^{-8}$
$\tau \rightarrow \mu\gamma$	$\sqrt{ Y_{\tau\mu} ^2 + Y_{\mu\tau} ^2}$	0.016
$\tau \rightarrow 3\mu$	$\sqrt{ Y_{\tau\mu}^2 + Y_{\mu\tau} ^2}$	$\lesssim 0.25$
muon $g - 2$	$\text{Re}(Y_{\mu\tau}Y_{\tau\mu})$	$(2.7 \pm 0.75) \times 10^{-3}$
muon EDM	$\text{Im}(Y_{\mu\tau}Y_{\tau\mu})$	$-0.8 \dots 1.0$
$\mu \rightarrow e\gamma$	$(Y_{\tau\mu}Y_{e\tau} ^2 + Y_{\mu\tau}Y_{\tau e} ^2)^{1/4}$	$< 3.4 \times 10^{-4}$

Table I: Constraints on flavor violating Higgs couplings to e , μ , τ for a Higgs mass $m_h = 125$ GeV and assuming that the flavor diagonal Yukawa couplings equal the SM values (see text for details). For the muon magnetic dipole moment we show the value of the couplings required to explain the observed Δa_μ (if this is used only as an upper bound one has $\sqrt{\text{Re}(Y_{\mu\tau}Y_{\tau\mu})} < 0.065$ at 95%CL).

diagrams, see Fig. 12 in Appendix A. The complete one loop and two loop expressions are given in Appendix A.

In the approximation $Y_{\mu\mu} \ll Y_{\tau\tau}$, only the first of the one-loop diagrams in Fig. 1 is relevant (in addition to the 2-loop diagrams). Using also $m_\mu \ll m_\tau \ll m_h$ and assuming $Y_{\mu\mu}$, $Y_{\tau\tau}$ to be real, the expressions for the one-loop Wilson coefficients c_L and c_R simplify to (this agrees with [24])

$$c_L^{\text{1loop}} \simeq \frac{1}{12m_h^2} Y_{\tau\tau} Y_{\tau\mu}^* \left(-4 + 3 \log \frac{m_h^2}{m_\tau^2} \right), \quad c_R^{\text{1loop}} \simeq \frac{1}{12m_h^2} Y_{\mu\tau} Y_{\tau\tau} \left(-4 + 3 \log \frac{m_h^2}{m_\tau^2} \right). \quad (13)$$

The 2-loop contributions are numerically

$$c_L^{2\text{loop}} = Y_{\tau\mu}^* (-0.082 Y_{tt} + 0.11) \frac{1}{(125\text{GeV})^2} = 0.055 Y_{\tau\mu}^* \frac{1}{(125\text{GeV})^2}, \quad (14)$$

where in the last step we used for the top Yukawa coupling $Y_{tt} = (Y_{tt})_{SM} = \bar{m}_t/v = 0.67$, and we have normalized the results to m_h for easier comparison. (By \bar{m}_t , we denote the top quark mass parameter in the $\overline{\text{MS}}$ renormalization scheme, $\bar{m}_t \simeq 164$ GeV.) The analytical form of the Wilson coefficient can be found in Appendix A. The same result applies to $c_R^{2\text{loop}}$ with the replacement $Y_{\tau\mu}^* \rightarrow Y_{\mu\tau}$. The 2-loop contribution consists is dominated by two terms, the one with the top quark in the loop and of a somewhat larger W contribution. They have opposite signs and thus part of W contributions is cancelled. The end result has an increased sensitivity to the precise value of Y_{tt} . For $Y_{tt} \simeq \bar{m}_t/v$ the 2-loop contribution is about four times as large as the 1-loop contribution, while for other values of Y_{tt} (e.g., $Y_{tt} \simeq -m_t/v$) the 2-loop contribution can be an order of magnitude larger. Note that we keep complete 2-loop expressions [36], including the finite terms, while in [20, 24] only the leading log term of the top loop contribution was kept. Numerically, this amounts to an $\mathcal{O}(1)$ difference.

In terms of the Wilson coefficients c_L and c_R , the rate for $\tau \rightarrow \mu\gamma$ is

$$\Gamma(\tau \rightarrow \mu\gamma) = \frac{\alpha m_\tau^5}{64\pi^4} (|c_L|^2 + |c_R|^2). \quad (15)$$

Using a Higgs mass $m_h = 125$ GeV and assuming $Y_{\tau\tau} = m_\tau/v$, $Y_{tt} = \bar{m}_t/v$, we can then translate the experimental bound $\text{BR}(\tau \rightarrow \mu\gamma) < 4.4 \times 10^{-8}$ [37] into a constraint $\sqrt{|Y_{\tau\mu}|^2 + |Y_{\mu\tau}|^2} < 1.6 \times 10^{-2}$ (see Table I). The bound is relaxed if $Y_{\tau\tau}$ and/or Y_{tt} are smaller than their SM values.

The expressions for $\mu \rightarrow e\gamma$ and $\tau \rightarrow e\gamma$ are obtained in an analogous way with the obvious replacements ($\tau \rightarrow \mu, \mu \rightarrow e$ for the first and $\mu \rightarrow e$ for the second in Eqs. (12), (13), (14), (15)). The experimental bound $\text{BR}(\mu \rightarrow e\gamma) < 2.4 \cdot 10^{-12}$ [37] then translates to $\sqrt{|Y_{\mu e}|^2 + |Y_{e\mu}|^2} < 3.6 \times 10^{-6}$ and $\text{BR}(\tau \rightarrow e\gamma) < 3.3 \times 10^{-8}$ [37] to a constraint $\sqrt{|Y_{\tau e}|^2 + |Y_{e\tau}|^2} < 1.4 \times 10^{-2}$ using the SM values for $Y_{\tau\tau}, Y_{\mu\mu}$, and Y_{tt} . The $\mu \rightarrow e\gamma$ bound is completely dominated by the two loop contribution, while for $\tau \rightarrow e\gamma$, the two loop and one loop contributions are comparable.

The decay $\mu \rightarrow e\gamma$ can also be used to place a bound on the combination $Y_{\mu\tau} Y_{\tau e}$ using

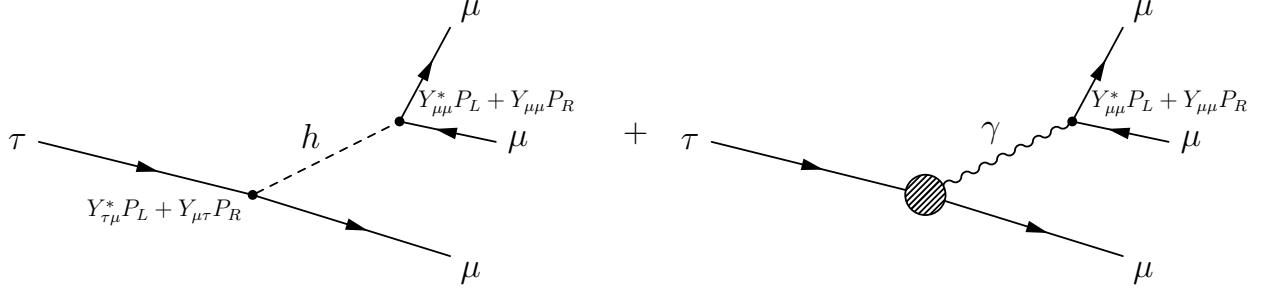


Figure 2: Diagrams leading to $\tau \rightarrow 3\mu$ decay. The tree level Higgs exchange contribution (left) is typically subdominant compared to higher-order contributions with the topology shown on the right. The blob represents loops of the form shown in Figs. 1 and 12.

the 1-loop Wilson coefficient (in agreement with [24])

$$c_L^{\text{1loop}} \simeq \frac{1}{8m_h^2} \frac{m_\tau}{m_\mu} Y_{\mu\tau}^* Y_{\tau e}^* \left(-3 + 2 \log \frac{m_h^2}{m_\tau^2} \right). \quad (16)$$

As before, c_R^{1loop} is obtained by replacing $Y_{\mu\tau}^* Y_{\tau e}^*$ by $Y_{\tau\mu} Y_{e\tau}$. The 2-loop contribution is proportional to $Y_{\mu e}$ and $Y_{e\mu}$. Setting them to zero, one obtains a bound $(|Y_{\tau\mu} Y_{e\tau}|^2 + |Y_{\mu\tau} Y_{\tau e}|^2)^{1/4} < 3.4 \times 10^{-4}$.

B. Constraints from $\tau \rightarrow 3\mu$, $\tau \rightarrow 3e$, $\mu \rightarrow 3e$

The decay $\tau \rightarrow 3\mu$ can be generated through tree level Higgs exchange, see the diagram in Fig. 2 (left). However, the diagram is suppressed not only by the flavor violating Yukawa couplings $Y_{\tau\mu}$ and $Y_{\mu\tau}$, but also by the flavor-conserving coupling $Y_{\mu\mu}$. It is thus subleading compared to the higher order contributions: the 1-loop diagrams of the form shown in Fig. 1 and 2-loop diagrams like the ones shown in Fig. 12 (for $\tau \rightarrow \mu\gamma$). These generate $\tau \rightarrow 3\mu$ if the outgoing gauge boson is off-shell and “decays” to a muon pair. This general topology is shown in the right part of Fig. 2.

Integrating out the Higgs, the heavy gauge bosons and the top quark, these contributions match onto an effective Lagrangian. The full effective Lagrangian is similar to the one in Eq. (A13) for $\mu \rightarrow e$ conversion, but with quarks replaced by muons. Since a full evaluation of the 2-loop contributions is beyond the scope of this work, we will estimate the $\tau \rightarrow 3\mu$ rate by including only the dimension 5 electromagnetic dipole contributions of the form given

in Eq. (12). For c_L and c_R , we use the same expressions as for $\tau \rightarrow \mu\gamma$, see Sec. III A and Appendix A. We evaluate these expressions at $q^2 = 0$. We have checked that the neglected contributions are numerically smaller than the dipole terms at one loop. At two loops, to the best of our knowledge, a full evaluation of all potentially relevant diagrams is not available.

The corresponding expression for the flavor violating partial width of the τ is

$$\Gamma(\tau \rightarrow 3\mu) \simeq \frac{\alpha^2 m_\tau^5}{6(2\pi)^5} \left| \log \frac{m_\mu^2}{m_\tau^2} - \frac{11}{4} \right| (|c_L|^2 + |c_R|^2), \quad (17)$$

where we have neglected terms additionally suppressed by the muon mass. The Wilson coefficients c_L and c_R are given approximately by Eqs. (13) and (14), with the 2-loop contribution dominating over the 1-loop one. In addition to (17) there are also contributions to the $\tau \rightarrow 3\mu$ rate from effective flavor violating Z vertices induced at 1-loop by flavor violating Higgs exchanges. These have the same scaling in terms of masses and the Yukawas as (17), but are found to be numerically an order of magnitude smaller [38]. We therefore neglect them in the following.

The experimental bound $\text{BR}(\tau \rightarrow 3\mu) < 2.1 \times 10^{-8}$ [39] translates into a constraint $\sqrt{|Y_{\tau\mu}^2 + |Y_{\mu\tau}|^2} < 0.25$ for $m_h = 125$ GeV and assuming that the diagonal Yukawa couplings $Y_{\tau\tau}$, $Y_{\mu\mu}$ and Y_{tt} have their Standard Model values. The decay $\tau \rightarrow 3\mu$ thus leads to a weaker limit on $Y_{\tau\mu}$, $Y_{\mu\tau}$ than $\tau \rightarrow \mu\gamma$, mainly because $\Gamma(\tau \rightarrow 3\mu)$ is suppressed by an additional power of α compared to $\Gamma(\tau \rightarrow \mu\gamma)$.

Similarly, the constraints on $Y_{\mu e}$, $Y_{e\mu}$, $Y_{\tau e}$, $Y_{e\tau}$ following from the processes $\mu \rightarrow 3e$ and $\tau \rightarrow 3e$ are weaker than the corresponding limits from $\mu \rightarrow e\gamma$ and $\tau \rightarrow e\gamma$. The bounds in Table I are obtained using the experimental results $\text{BR}(\mu \rightarrow 3e) < 1.0 \times 10^{-12}$ [40] and $\text{BR}(\tau \rightarrow 3e) < 2.7 \times 10^{-8}$ [41]. We have also considered the process $\tau \rightarrow e\mu\mu$, but found that it yields a weaker limit than $\tau \rightarrow 3e$, mainly because of the smaller phase space.

C. Constraints from muonium–antimuonium oscillations

A μ^+e^- bound state (called muonium M) can oscillate into an $e^+\mu^-$ bound state (antimuonium \bar{M}) through the diagram in Fig. 3. The time-integrated $M \rightarrow \bar{M}$ conversion probability is constrained by the MACS experiment at PSI [42] to be below $P(M \rightarrow \bar{M}) < 8.3 \times 10^{-11}/S_B$, where the correction factor $S_B \leq 1$ accounts for the splitting of muonium states in the magnetic field of the detector. It depends on the Lorentz structure

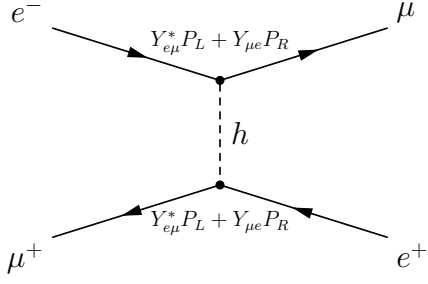


Figure 3: Diagram leading to muonium–antimuonium oscillations.

of the conversion operator and varies between $S_B = 0.35$ for $(S \pm P) \times (S \pm P)$ operators and $S_B = 0.9$ for $P \times P$ operators [42]. Conservatively, we use the smallest value $S_B = 0.35$ throughout. Since we will find that $M\text{--}\bar{M}$ oscillation constraints are much weaker than those from $\mu \rightarrow e\gamma$ and $\mu \rightarrow e$ conversion, this approximation suffices for illustrative purposes.

The theoretical prediction for the $M \rightarrow \bar{M}$ conversion rate is governed by the mixing matrix element (see, e.g., [43])

$$\mathcal{M}_{\bar{M}M} = \langle \uparrow_\mu \downarrow_{\bar{e}} - \downarrow_\mu \uparrow_{\bar{e}} \mid \frac{[\bar{\mu}(Y_{e\mu}^* P_L + Y_{\mu e} P_R)e] [\bar{\mu}(Y_{e\mu}^* P_L + Y_{\mu e} P_R)e]}{2m_h^2} \mid \uparrow_e \downarrow_{\bar{\mu}} - \downarrow_e \uparrow_{\bar{\mu}} \rangle, \quad (18)$$

where \uparrow_X and \downarrow_X are the spin orientations of particle X . We can work in the non-relativistic limit here. For a contact interaction, the spatial wave function of muonium, $\phi_{1s} = \exp(-r/a_M)/[\pi a_M^3]^{1/2}$, only needs to be evaluated at the origin. (Here r is the electron–antimuon distance and $a_M = (m_e + m_\mu)/(m_e m_\mu \alpha)$ is the muonium Bohr radius.) The resulting mass splitting between the two mass eigenstates of the mixed $M\text{--}\bar{M}$ system is [43],

$$\Delta M = 2 |\mathcal{M}_{\bar{M}M}| = \frac{|Y_{\mu e} + Y_{e\mu}^*|^2}{2\pi a^3 m_h^2}, \quad (19)$$

and the time-integrated conversion probability is

$$P(M \rightarrow \bar{M}) = \int_0^\infty dt \Gamma_\mu \sin^2(\Delta M t) e^{-\Gamma_\mu t} = \frac{2}{\Gamma_\mu^2/(\Delta M)^2 + 4}. \quad (20)$$

The bound from the MACS experiment [42] then translates into $|Y_{\mu e} + Y_{e\mu}^*| < 0.079$.

D. Constraints from magnetic dipole moments

The CP conserving and CP violating parts of the diagram in Fig. 4 generate magnetic and electric dipole moments of the muon, respectively. Since the experimental value of the

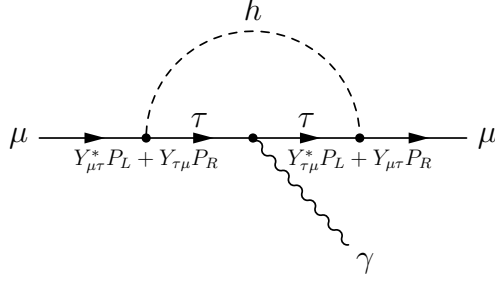


Figure 4: A diagram contributing to the anomalous magnetic moment $g - 2$ of the muon through FV couplings of the Higgs to $\tau\mu$.

magnetic dipole moment, $g_\mu - 2$, is above the SM prediction at more than 3σ , also the preferred value for the flavor violating Higgs couplings will be nonzero.

The FV contribution to $(g - 2)_\mu$ due to the τ -Higgs loop in Fig. 4 is (neglecting terms suppressed by m_μ/m_τ or m_τ/m_h)

$$a_\mu \equiv \frac{g_\mu - 2}{2} \simeq \frac{\text{Re}(Y_{\mu\tau} Y_{\tau\mu})}{8\pi^2} \frac{m_\mu m_\tau}{2m_h^2} \left(2 \log \frac{m_h^2}{m_\tau^2} - 3 \right), \quad (21)$$

in agreement with [24]. The discrepancy between the measured value of a_μ and the one predicted by the Standard Model [39, 44],

$$\Delta a_\mu \equiv a_\mu^{\text{exp}} - a_\mu^{\text{SM}} = (2.87 \pm 0.63 \pm 0.49) \times 10^{-9}, \quad (22)$$

could thus be explained if there are FV Higgs interactions of the size

$$\text{Re}(Y_{\mu\tau} Y_{\tau\mu}) \simeq (2.7 \pm 0.75) \times 10^{-3}, \quad (23)$$

(for the definition of the Yukawa couplings see Eq. (1)). This explanation of Δa_μ requires $Y_{\mu\tau} \sim Y_{\tau\mu}$ to be a factor of a few bigger than the SM value of the diagonal Yukawa, m_τ/v , and is in tension with limits from $\tau \rightarrow \mu\gamma$.³ It is in further tension with the LHC limit extracted in Sec. V of this paper.

The measured Δa_μ could in principle also be explained by an enhanced flavor conserving coupling of the muon to the Higgs if $Y_{\mu\mu} \sim 0.15 \sim 280 m_\mu/v$. However, in this case $h \rightarrow \mu\mu$

³ If the two loop contribution to $\tau \rightarrow \mu\gamma$ is suppressed, e.g. due to a modification of the top Yukawa coupling, which could lead to significant cancellation between the 2-loop top and W diagrams, there is a small region of parameter space in which flavor violating Higgs couplings could explain the $(g - 2)_\mu$ discrepancy without being ruled out by the one loop $\tau \rightarrow \mu\gamma$ constraint. We will, however, see below that even this case is disfavored by the LHC limit derived in this paper (see Sec. V A).

decays would be enhanced to a level that is already ruled out by the searches at the LHC: From the search for the MSSM neutral Higgs boson one obtains a bound $\sigma(gg \rightarrow h \rightarrow \mu\mu) \lesssim 30 \times \sigma(gg \rightarrow h \rightarrow \mu\mu)_{\text{SM}}$ or $Y_{\mu\mu} \lesssim 5.5 m_\mu/v$ [45].

E. Constraints from electric dipole moments

If the flavor violating Yukawa couplings in Fig. 4 are complex, the diagram shown there generates also an *electric* dipole moment (EDM) for the muon. The relevant term in the effective Lagrangian is

$$\mathcal{L}_{\text{EDM}} = -\frac{i}{2} d_\mu (\bar{\mu} \sigma^{\alpha\beta} \gamma^5 \mu) F_{\alpha\beta}, \quad (24)$$

with the electric dipole moment given by (neglecting the terms suppressed by m_μ/m_τ or m_τ/m_h)

$$d_\mu \simeq -\frac{\text{Im}(Y_{\mu\tau} Y_{\tau\mu})}{16\pi^2} \frac{e m_\tau}{2m_h^2} \left(2 \log \frac{m_h^2}{m_\tau^2} - 3 \right), \quad (25)$$

in agreement with [24]. The experimental constraint $-10 \times 10^{-20} e \text{ cm} < d_\mu < 8 \times 10^{-20} e \text{ cm}$ [37] translates into the rather weak limit $-0.8 \lesssim \text{Im}(Y_{\mu\tau} Y_{\tau\mu}) \lesssim 1.0$.

A similar diagram with electrons instead of muons on the external legs also contributes to the electron EDM, d_e . The experimental constraint $|d_e| < 0.105 \times 10^{-26} e \text{ cm}$ [37] translates into $|\text{Im}(Y_{e\tau} Y_{\tau e})| < 1.1 \times 10^{-8}$ for a tau running in the loop, and into $|\text{Im}(Y_{e\mu} Y_{\mu e})| < 9.8 \times 10^{-8}$ for a muon running in the loop.

F. Constraints from $\mu \rightarrow e$ conversion in nuclei

Very stringent constraints on the FV Yukawa couplings $Y_{\mu e}$ and $Y_{e\mu}$ come from experimental searches for $\mu \rightarrow e$ conversion in nuclei. The relevant tree-level and one-loop diagrams with one insertion of the FV Yukawa coupling are shown in Fig. 5. An effective scalar interaction arises already at tree level from the first diagram in Fig. 5, while vector and electromagnetic dipole contributions arise at one loop level. We give complete expressions for the tree level and one loop contributions in Appendix A 3. There are also two-loop contributions, similar to the ones discussed in Sec. III A in the context of $\mu \rightarrow e\gamma$. Numerically, the two-loop contributions are larger than the one loop ones because they are not

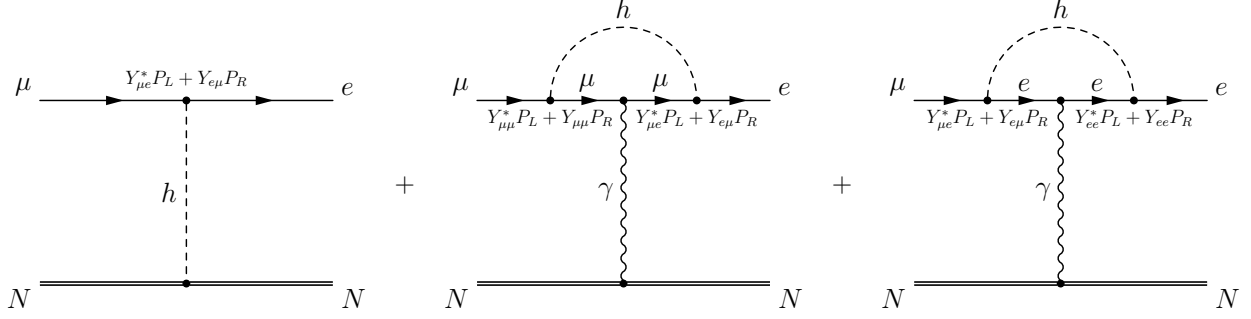


Figure 5: Tree-level and one-loop diagrams contributing to $\mu \rightarrow e$ conversion in nuclei via the flavor violating Higgs Yukawa couplings $Y_{\mu e}$ and $Y_{e\mu}$. In addition, we also include numerically important two-loop diagrams, see Appendix A 3 for details.

suppressed by the small $Y_{\mu\mu}$ coupling but only by Y_{tt} or the weak gauge coupling. They are in fact comparable to the tree level contribution. Here, we always assume the diagonal Yukawa couplings to have their SM values. With this assumption, the tree level term is very sensitive to the strangeness content of the nucleon.

The bounds on the Yukawa couplings $Y_{e\mu}$ and $Y_{\mu e}$ from $\mu \rightarrow e$ conversion in nuclei, including tree level, one-loop and two-loop contributions, are listed in Table I.

One could potentially also obtain interesting limits on $|Y_{e\tau}|$ and $|Y_{\tau e}|$ from $\mu \rightarrow e$ conversion in nuclei, even though this requires diagrams proportional to *two* FV Yukawa couplings, because the other constraints on these couplings are weak. The combinations $Y_{e\tau}Y_{\tau\mu}$, $Y_{e\tau}Y_{\mu\tau}^*$, $Y_{\tau e}^*Y_{\tau\mu}$ and $Y_{\tau e}^*Y_{\mu\tau}^*$ are constrained by $\mu \rightarrow e$ conversion through 1-loop diagrams similar to the ones shown in Fig. 5, but with a τ running in the loop (see Eq. (A16)). In the simplest case, $Y_{e\tau} = Y_{\tau e}$, $Y_{\mu\tau} = Y_{\tau\mu}$, with all Yukawa couplings real, the constraint is $Y_{e\tau}Y_{\mu\tau} \lesssim 10^{-6}$. This is almost, but not quite, competitive with the bound following from $\tau \rightarrow e\gamma$ and $\tau \rightarrow \mu\gamma$ decays, see Table I.

G. LEP constraints

The Large Electron–Positron collider (LEP) is indirectly sensitive to the flavor violating Yukawa couplings $Y_{\ell e}$ and $Y_{e\ell}$ (with $\ell = \mu, \tau$) through the process $e^+e^- \rightarrow \ell^+\ell^-$, mediated by a t -channel Higgs. The relevant observables here are the total cross sections $\sigma(e^+e^- \rightarrow \ell^+\ell^-)$ and the forward–backward asymmetry of the final state leptons, both of which were measured

as a function of the center-of-mass energy \sqrt{s} with uncertainties of order several per cent [46]. However, since the new physics contribution to $\sigma(e^+e^- \rightarrow \ell^+\ell^-)$ is proportional to four powers of the off-diagonal Yukawa couplings, LEP limits cannot compete with constraints from flavor-violating decays like $\tau \rightarrow \mu\gamma$ and $\mu \rightarrow e\gamma$ and with the LHC constraints we derive in Section V. While a full derivation of LEP limits, including a careful treatment of the interference between Standard Model and non-standard contributions as well as a fit to the data points given in [46] is beyond the scope of this work, we have estimated that flavor-violating couplings $\sqrt{|Y_{\ell e}|^2 + |Y_{e\ell}|^2} \lesssim \text{few} \times 10^{-1}$ are excluded by LEP.

H. Allowed branching ratios for lepton flavor violating Higgs decays

In Fig. 6 we collect the above constraints on the values of $|Y_{e\tau}|$, $|Y_{\tau e}|$ (upper left panel), $|Y_{e\mu}|$, $|Y_{\mu e}|$ (upper right panel) and $|Y_{\mu\tau}|$, $|Y_{\tau\mu}|$ (lower panel) and relate them to the predicted branching ratios for $h \rightarrow e\tau$, $h \rightarrow \tau e$ and $h \rightarrow \mu\tau$. The latter are given by

$$\text{BR}(h \rightarrow \ell^\alpha \ell^\beta) = \frac{\Gamma(h \rightarrow \ell^\alpha \ell^\beta)}{\Gamma(h \rightarrow \ell^\alpha \ell^\beta) + \Gamma_{\text{SM}}}, \quad (26)$$

where $\ell^\alpha, \ell^\beta = e, \mu, \tau$, $\ell^\alpha \neq \ell^\beta$. The decay width $\Gamma(h \rightarrow \ell^\alpha \ell^\beta)$, in turn, is

$$\Gamma(h \rightarrow \ell^\alpha \ell^\beta) = \frac{m_h}{8\pi} (|Y_{\ell^\beta \ell^\alpha}|^2 + |Y_{\ell^\alpha \ell^\beta}|^2), \quad (27)$$

and the SM Higgs width is $\Gamma_{\text{SM}} = 4.1$ MeV for a 125 GeV Higgs boson [47]. In the panels of Fig. 6 we are assuming that at most one of non-standard decay mode of the Higgs is significant compared to the SM decay width.

From Fig. 6 we see that given current bounds from $\tau \rightarrow \mu\gamma$ and $\tau \rightarrow e\gamma$, branching fractions for $h \rightarrow \tau\mu$ or $h \rightarrow \tau e$ in the neighborhood of 10% are allowed. This is well within the reach of the LHC as we shall show in Sec. V. The allowed sizes of these two decay widths are comparable to the sizes of decay widths into nonstandard decay channels (such as the invisible decay width) that are allowed by global fits [48]. If there is no significant negative contribution to Higgs production through gluon fusion, one has $\text{BR}(h \rightarrow \text{invisible}) \lesssim 20\%$, while allowing for arbitrarily large modifications of gluon and photon couplings to the Higgs leads to the constraint $\text{BR}(h \rightarrow \text{invisible}) \lesssim 65\%$ [48]. These two bounds apply without change also to $\text{BR}(h \rightarrow \tau\mu)$, $\text{BR}(h \rightarrow \tau e)$ and $\text{BR}(h \rightarrow e\mu)$.

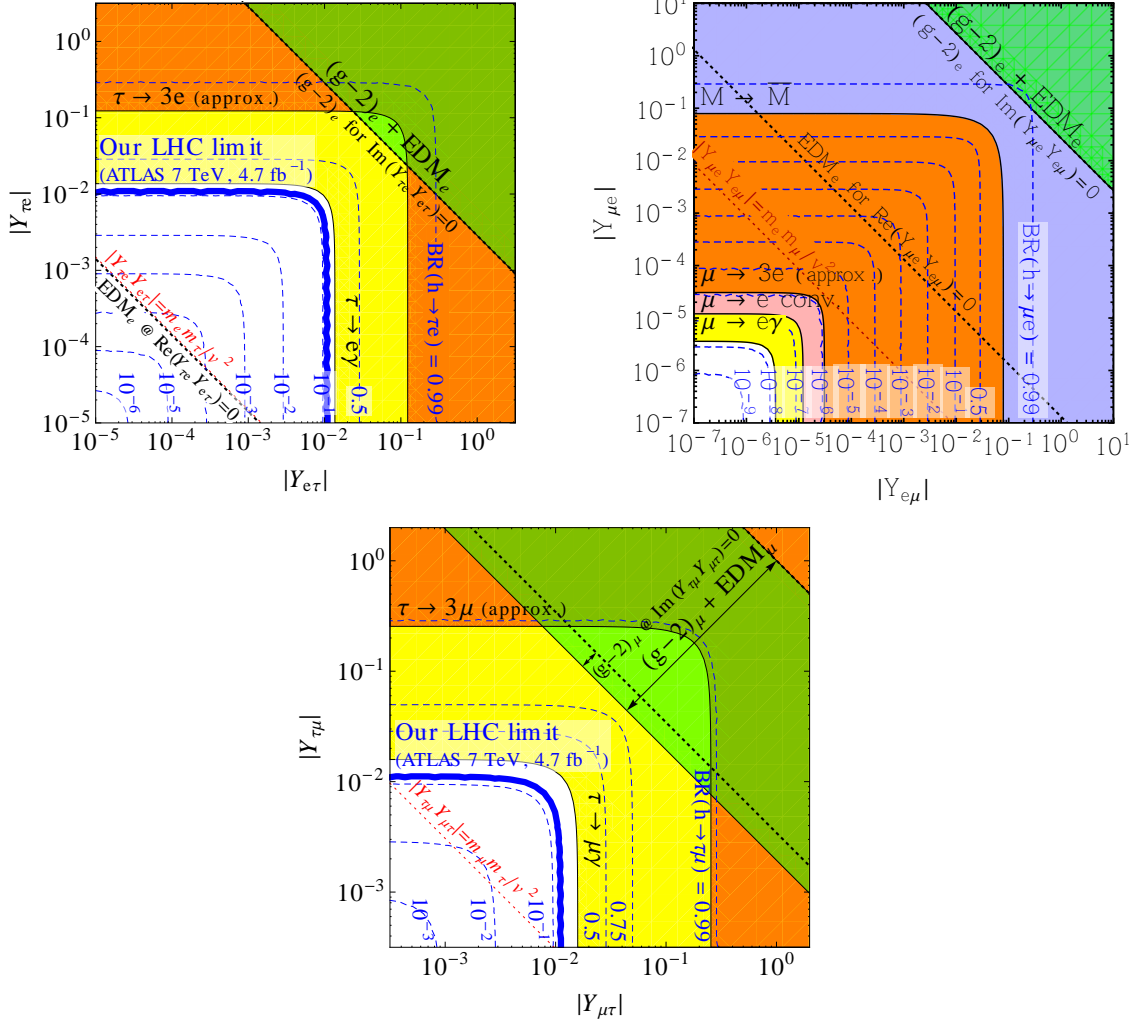


Figure 6: Constraints on the flavor violating Yukawa couplings $|Y_{e\tau}|$, $|Y_{\tau e}|$ (upper left panel), $|Y_{e\mu}|$, $|Y_{\mu e}|$ (upper right panel) and $|Y_{\mu\tau}|$, $|Y_{\tau\mu}|$ (lower panel) of a 125 GeV Higgs boson. The diagonal Yukawa couplings are approximated by their SM values. Thin blue dashed lines are contours of constant BR for $h \rightarrow \tau e$, $h \rightarrow \mu e$ and $h \rightarrow \tau \mu$, respectively, whereas thick blue lines are the LHC limits derived in Sec. V A. (These limits could be greatly improved with dedicated searches on existing LHC data, see Sec. V C.) Shaded regions show the constraints discussed in Sec. III as indicated in the plots. Note that $g - 2$ [EDM] searches (diagonal black dotted lines) are only sensitive to parameter combinations of the form $\text{Re}(Y_{\alpha\beta}Y_{\beta\alpha})$ [$\text{Im}(Y_{\alpha\beta}Y_{\beta\alpha})$]. We also show limits from a combination of $g - 2$ and EDM searches with marginalization over the complex phases of the Yukawa couplings ($g - 2$ and EDM) (green shaded regions). Note that $(g - 2)_\mu$ provides upper and lower limits (as indicated by the double-sided arrows in the lower panel) if the discrepancy between the measurement and the SM prediction [39, 44] is taken into account. The thin red dotted lines show rough naturalness limits $Y_{ij}Y_{ji} \lesssim m_i m_j / v^2$ (see Sec. II).

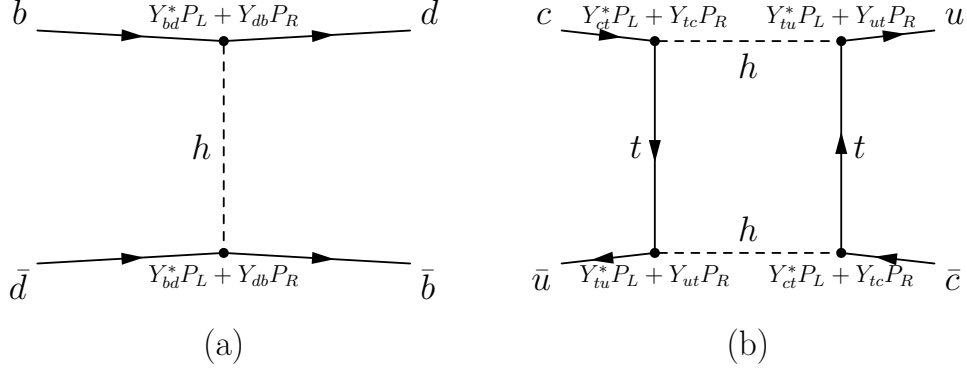


Figure 7: Two representative diagrams through which flavor violating Higgs Yukawa couplings can contribute to neutral meson mixing.

In contrast to decays involving a τ lepton, the branching ratio for $h \rightarrow e\mu$ is extremely well constrained by $\mu \rightarrow e\gamma$, $\mu \rightarrow 3e$ and $\mu \rightarrow e$ conversion bounds, and is required to be below $\text{BR}(h \rightarrow e\mu) \lesssim 2 \times 10^{-8}$, well beyond the reach of the LHC.

IV. HADRONIC FLAVOR VIOLATING DECAYS OF THE HIGGS

We next consider flavor violating decays of the Higgs to quarks. We first discuss two-body decays to light quarks, $h \rightarrow \bar{b}d$, $\bar{b}s$, $\bar{s}d$, $\bar{c}u$, and then turn to FV three body decays mediated by an off-shell top, $h \rightarrow \bar{t}^*c \rightarrow W\bar{b}c$ and $h \rightarrow \bar{t}^*u \rightarrow W\bar{b}u$ as well as FV top decays to $t \rightarrow ch$ and $t \rightarrow uh$. Our limits are summarized in Table II.

A. Flavor violating Higgs decays into light quarks

Flavor violating Higgs couplings to quarks can generate flavor changing neutral currents (FCNCs) at tree level, see Fig. 7 (a), and are thus well constrained by the measured $B_{d,s} - \bar{B}_{d,s}$, $K^0 - \bar{K}^0$ and $D^0 - \bar{D}^0$ mixing rates. Integrating out the Higgs generates an effective weak Hamiltonian, which for $B_d - \bar{B}_d$ mixing is

$$H_{\text{eff}} = C_2^{db} (\bar{b}_R d_L)^2 + \tilde{C}_2^{db} (\bar{b}_L d_R)^2 + C_4^{db} (\bar{b}_L d_R) (\bar{b}_R d_L). \quad (28)$$

Technique	Coupling	Constraint
D^0 oscillations [49]	$ Y_{uc} ^2, Y_{cu} ^2$	$< 5.0 \times 10^{-9}$
	$ Y_{uc}Y_{cu} $	$< 7.5 \times 10^{-10}$
B_d^0 oscillations [49]	$ Y_{db} ^2, Y_{bd} ^2$	$< 2.3 \times 10^{-8}$
	$ Y_{db}Y_{bd} $	$< 3.3 \times 10^{-9}$
B_s^0 oscillations [49]	$ Y_{sb} ^2, Y_{bs} ^2$	$< 1.8 \times 10^{-6}$
	$ Y_{sb}Y_{bs} $	$< 2.5 \times 10^{-7}$
K^0 oscillations [49]	$\text{Re}(Y_{ds}^2), \text{Re}(Y_{sd}^2)$	$[-5.9 \dots 5.6] \times 10^{-10}$
	$\text{Im}(Y_{ds}^2), \text{Im}(Y_{sd}^2)$	$[-2.9 \dots 1.6] \times 10^{-12}$
	$\text{Re}(Y_{ds}^*Y_{sd})$	$[-5.6 \dots 5.6] \times 10^{-11}$
	$\text{Im}(Y_{ds}^*Y_{sd})$	$[-1.4 \dots 2.8] \times 10^{-13}$
single-top production [50]	$\sqrt{ Y_{tc}^2 + Y_{ct} ^2}$	< 3.7
	$\sqrt{ Y_{tu}^2 + Y_{ut} ^2}$	< 1.6
$t \rightarrow hj$ [51]	$\sqrt{ Y_{tc}^2 + Y_{ct} ^2}$	< 0.34
	$\sqrt{ Y_{tu}^2 + Y_{ut} ^2}$	< 0.34
D^0 oscillations [49]	$ Y_{ut}Y_{ct} , Y_{tu}Y_{tc} $	$< 7.6 \times 10^{-3}$
	$ Y_{tu}Y_{ct} , Y_{ut}Y_{tc} $	$< 2.2 \times 10^{-3}$
	$ Y_{ut}Y_{tu}Y_{ct}Y_{tc} ^{1/2}$	$< 0.9 \times 10^{-3}$
neutron EDM [37, 52]	$ \text{Im}(Y_{ut}Y_{tu}) $	$< 4.3 \times 10^{-7}$
	$ \text{Im}(Y_{ct}Y_{tc}) $	$< 5.0 \times 10^{-4}$

Table II: Constraints on flavor violating Higgs couplings to quarks. We have assumed a Higgs mass $m_h = 125$ GeV, and we have taken the diagonal Yukawa couplings at their SM values.

Here we use the same notation for the Wilson coefficients as in [49] and display only nonzero contributions, which are

$$C_2^{db} = -\frac{(Y_{db}^*)^2}{2m_h^2}, \quad \tilde{C}_2^{db} = -\frac{(Y_{bd}^2)^2}{2m_h^2}, \quad C_4^{db} = -\frac{Y_{bd}Y_{db}^*}{m_h^2}. \quad (29)$$

The results for $B_s - \bar{B}_s$, $K^0 - \bar{K}^0$ and $D^0 - \bar{D}^0$ mixing are obtained in the same way with the obvious quark flavor replacements. We can now translate the bounds on the above Wilson coefficients obtained in [49] into constraints on the combinations of flavor violating Higgs couplings as summarized in Table II. We see that all Yukawa couplings involving only u ,

d , s , c , or b quarks have to be tiny. The weakest constraints are those in the b - s sector, where flavor violating Yukawa couplings $\lesssim 10^{-3}$ are still allowed. This would correspond to $\text{BR}(h \rightarrow bs) \sim 2 \times 10^{-3}$, which is still far too small to be observed at the LHC because of the large QCD backgrounds.

B. Higgs decays through off-shell top and top decays to Higgs

Among the flavor violating Higgs couplings to quarks, the most promising place for new physics to hide are processes involving top quarks, such as the 3-body decay $h \rightarrow (t^* \rightarrow Wb)q$. Here, q denotes either a charm quark or an up quark. The corresponding FV Yukawa couplings contribute at one loop to $D - \bar{D}$ mixing through diagrams of the form of Fig. 7 (b). The corresponding Wilson coefficients in the effective Hamiltonian (28) are

$$C_1^{uc} = \frac{1}{4} \frac{1}{16\pi^2} \frac{S_1^H(x_{tH})}{m_h^2} (Y_{ct} Y_{ut}^*)^2, \quad \tilde{C}_1^{uc} = \frac{1}{4} \frac{1}{16\pi^2} \frac{S_1^H(x_{tH})}{m_h^2} (Y_{tc}^* Y_{tu})^2, \quad (30)$$

$$C_2^{uc} = -\frac{1}{4} \frac{1}{16\pi^2} \frac{S_2^H(x_{tH})}{m_h^2} (Y_{tc}^* Y_{ut}^*)^2, \quad \tilde{C}_2^{uc} = -\frac{1}{4} \frac{1}{16\pi^2} \frac{S_2^H(x_{tH})}{m_h^2} (Y_{ct} Y_{tu})^2, \quad (31)$$

$$C_4^{uc} = -\frac{1}{2} \frac{1}{16\pi^2} \frac{S_2^H(x_{tH})}{m_h^2} (Y_{ct} Y_{tu}) (Y_{tc}^* Y_{ut}^*), \quad C_5^{uc} = -\frac{1}{16\pi^2} \frac{S_1^H(x_{tH})}{m_h^2} (Y_{ct} Y_{ut}^*) (Y_{tc}^* Y_{tu}), \quad (32)$$

where

$$S_1^H(x) = \frac{x^2 - 1 - 2x \log x}{2(x-1)^3}, \quad S_2^H(x) = \frac{2x[2 - 2x + (1+x) \log x]}{(x-1)^3}, \quad (33)$$

and $x_{tH} \equiv m_t^2/m_h^2$. Note that now also the operators $Q_{1,5}^{uc}, \tilde{Q}_1^{uc}$ (in the notation of [49]) have non-zero Wilson coefficients. By requiring that each individual operator is consistent with its $D - \bar{D}$ mixing constraint, we derive the limits shown in the last part of Table II. The constraints are much weaker than those on FV Higgs couplings involving only light quarks.

Strong constraints on Y_{qt} and Y_{tq} are also obtained from the non-observation of anomalous single top production. The flavor violating chromomagnetic operators

$$\mathcal{L}_{\text{single top}} \supset \frac{g_s}{m_h} \bar{t} \sigma^{\mu\nu} (\kappa_{tqg,L} P_L + \kappa_{tqg,R} P_R) \frac{\lambda^a}{2} q G_{\mu\nu}^a, \quad (34)$$

are generated through loop diagrams similar to Fig. 1, but with leptons replaced by quarks and the photon replaced by a gluon. Here g_s is the strong coupling constant, λ^a are the Gell-Mann matrices, $G_{\mu\nu}^a$ is the gluon field strength tensor, and $\kappa_{tqg,L}, \kappa_{tqg,R}$ are dimensionless

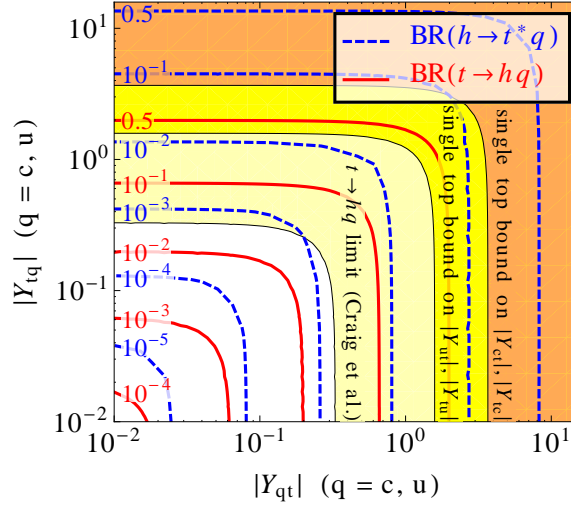


Figure 8: Predictions for various flavor changing neutral current (FCNC) processes mediated by the flavor violating Yukawa couplings Y_{ct} , Y_{tc} or Y_{ut} , Y_{tu} of a 125 GeV Higgs boson. Where appropriate, we have approximated the diagonal Yukawa couplings by their Standard Model values. Blue dashed contours indicate the branching ratio for $h \rightarrow t^* q$, red solid contours the one for $t \rightarrow h q$ (where q denotes a charm or up quark). The light yellow region shows a recent limit on $t \rightarrow hc$ (or hu) from an LHC multi-lepton search [51].

effective coupling constants which depend on Y_{qt} and Y_{tq} according to

$$\kappa_{tqg,L} = \frac{m_t m_h}{8\pi^2} F(m_t, m_t, 0, q^2 = 0, Y^\dagger), \quad (35)$$

with the loop function F given in Eq. (A3). The analogous expression for $\kappa_{tqg,R}$ is obtained by replacing $Y_{tq}^* \rightarrow Y_{qt}$ and $Y_{tt} \rightarrow Y_{tt}^*$ in F . Note that in (35) we have assumed an EFT description with an on-shell gluon. Since $m_h \sim m_t$ this is only approximate, but we have checked that varying $q^2 \in [0, m_t^2]$ changes the bounds on Y_{tq} , Y_{qt} only by $\sim 10\%$. We have also made the approximation $m_q \rightarrow 0$, which is obeyed even much better. Limits on $\kappa_{tqg,L}$, $\kappa_{tqg,R}$ have been derived by the CDF and DØ collaborations [50, 53] and most recently by ATLAS [54]. In the notation of [54], we have $|\kappa_{tqf}|/\Lambda \equiv \sqrt{|\kappa_{tqg,L}|^2 + |\kappa_{tqg,R}|^2}/(\sqrt{2}m_h)$. We obtain the constraints

$$\sqrt{|Y_{tc}^2| + |Y_{ct}|^2} < 3.7, \quad \sqrt{|Y_{tu}^2| + |Y_{ut}|^2} < 1.6, \quad (36)$$

We now translate these bounds into constraints on the $h \rightarrow (\bar{t}^* \rightarrow W\bar{b})q$ decay width, which is given by (setting $m_{b,q} = 0$)

$$\frac{d^2\Gamma(h \rightarrow \bar{t}^*q)}{dm_{12}^2 dm_{23}^2} = \frac{3g^2|V_{tb}|^2}{64(2\pi)^3 m_W^2 m_h^3} \frac{1}{(m_{23}^2 - m_t^2)^2} \left[m_{12}^2 (2m_W^2 - m_{23}^2) (m_t^2 |Y_{qt}|^2 - m_{23}^2 |Y_{tq}|^2) \right. \\ \left. + (m_h^2 - m_{23}^2) (m_{23}^2 - m_W^2) (2m_W^2 |Y_{tq}|^2 + m_t^2 |Y_{qt}|^2) \right], \quad (37)$$

where $V_{tb} \simeq 1$ is a CKM matrix element. The branching ratio for $h \rightarrow t^*c$ can be as large as $\mathcal{O}(10^{-3})$, and the one for $h \rightarrow t^*u$ can be few $\times 10^{-4}$ as shown in Fig. 8.

If the decay $h \rightarrow (t^* \rightarrow Wb)c$ is non-negligible, so is the related non-standard top quark decay mode $t \rightarrow hc$, the rate for which is given by (neglecting the charm mass)

$$\Gamma(t \rightarrow hc) = \frac{|Y_{ct}|^2 + |Y_{tc}|^2}{32\pi} \frac{(m_t^2 - m_h^2)^2}{m_t^3}. \quad (38)$$

Branching ratios for $t \rightarrow hc$ of several tens of per cent are perfectly viable and can be searched for, e.g. in the multi-lepton or $t \rightarrow b\bar{b}c$ channels. In fact, the strongest hint on Higgs couplings to tc are already coming from a CMS multi-lepton search which was recast in [51] to search for $t \rightarrow hc$, giving a bound of 2.7% on the branching fraction of a top into a Higgs and a charm or up quark. This yields a limit of $\sqrt{|Y_{ti}|^2 + |Y_{it}|^2} < 0.34$ for $i = u$ or c (see Fig. 8).

We have also calculated the branching ratios for the loop-induced processes $t \rightarrow q\gamma$, $t \rightarrow qg$ and $t \rightarrow qZ$ ($q = u, c$), which are in principle sensitive to $|Y_{qt}|$ and $|Y_{tq}|$, but have found that even for $|Y_{qt}|, |Y_{tq}| \sim \mathcal{O}(1)$ the current experimental bounds are satisfied [55].

In the above we have assumed that the weak phases of Y_{ut} and Y_{tu} are negligibly small. Otherwise an unacceptably large contribution to the neutron EDM is generated at 1-loop level with top and Higgs running in the loop. Eq. (25) with the replacements $m_\tau \rightarrow m_t$, and $Y_{\mu\tau}Y_{\tau\mu} \rightarrow Y_{ut}Y_{tu}$ gives the u -quark EDM $d_u = e\tilde{d}_u$, from which one can calculate the neutron EDM d_n [56]. Using the 90% CL experimental bound $d_n < 0.29 \times 10^{-25} e \text{ cm}$ [37] together with the estimate for the relation between the quark and neutron EDMs, Eq. (3.62) of [56], one obtains $|\text{Im}Y_{ut}Y_{tu}| \lesssim 4.4 \times 10^{-8}$. To obtain this limit we have used the full one-loop expression for the quark EDMs rather than the approximation Eq. (25). For simplicity, we have neglected the contributions from chromomagnetic operators, which are similar in magnitude to the terms we keep. Including chromomagnetic terms and taking into account renormalization group running as well as using a conservative estimate of hadronic matrix elements, the authors of [52] obtain $|\text{Im}Y_{ut}Y_{tu}| < 4.3 \times 10^{-7}$ and $|\text{Im}Y_{ct}Y_{tc}| < 5.0 \times 10^{-4}$.

We see that the limit on $|\text{Im}Y_{ut}Y_{tu}|$ is much more stringent than the bounds on the absolute values of the same FV Yukawa couplings. In contrast, our estimates for the bounds from charm running in the loop, $|\text{Im}Y_{uc}Y_{cu}| < 1.6 \times 10^{-7}$, and from d -quark EDMs generated by the b -quark and s -quark running in the loop, $|\text{Im}Y_{ab}Y_{bd}| < 6.4 \times 10^{-8}$ and $|\text{Im}Y_{ds}Y_{sd}| < 1.2 \times 10^{-6}$, respectively, are less stringent than the bounds from meson mixing, Table II.

V. SEARCHING FOR FLAVOR VIOLATING HIGGS DECAYS AT THE LHC

We next discuss possible search strategies for flavor violating Higgs decays at the LHC, focusing on the $h \rightarrow \tau\mu$ and $h \rightarrow \tau e$ decays. As shown in Fig. 6, these are among the least constrained of the couplings discussed in this paper, with a potential to modify the Higgs branching fractions significantly. They are sensitive to new particles with flavor violating couplings or to a secondary mechanisms of electroweak symmetry breaking such as additional Higgs doublets, and are thus good probes of new physics. Furthermore, they are also interesting final states as far as the potential for searches at the LHC is concerned.

The decay $h \rightarrow \tau\mu$ is quite similar to the standard model $h \rightarrow \tau\tau$ decay with one of the tau leptons decaying to a muon. This implies that existing SM Higgs searches, with only small or no modifications at all, can already be used to place bounds on the flavor violating decay. We thus first extract limits on $h \rightarrow \tau\mu$ and $h \rightarrow \tau e$ decays from an existing $h \rightarrow \tau\tau$ search in ATLAS. We then discuss how modifications to the $\tau\tau$ search can lead to significantly improved sensitivity to flavor violating Higgs decays.

A. Extracting a bound on Higgs decays to $\tau\mu$ and τe

We use the existing ATLAS search for $h \rightarrow \tau\tau$ in the fully leptonic channel [57] to place bounds on the $h \rightarrow \tau\mu$ and $h \rightarrow \tau e$ branching fractions. The reason we use fully leptonic events is that we can simulate the detector response to them more accurately than for events involving hadronic taus. It should, however, be noted that in the SM $h \rightarrow \tau\tau$ search in ATLAS, semi-hadronic events are about as sensitive as fully leptonic ones [57], and in CMS, the semi-hadronic mode provides even stronger limits [27]. The analysis in [57] uses the collinear approximation to reconstruct the $\tau\tau$ invariant mass, i.e. it is assumed that the neutrino and the charged lepton emitted in tau decay are collinear. This approach is less

optimized for $h \rightarrow \tau\tau$ than the maximum-likelihood method employed by CMS [58], but it is more model independent so that a substantial fraction of $h \rightarrow \tau\mu$ or $h \rightarrow \tau e$ decays would pass the cuts.⁴ For simplicity we only use the ATLAS cuts optimized for Higgs production in vector boson fusion (VBF) since this channels provides the best sensitivity [57].

To derive limits we have generated 50,000 $pp \rightarrow 2j + (h \rightarrow \tau\mu)$ Monte Carlo events using MadGraph 5 v1.4.6 [59] for parton level event generation, Pythia 6.4 for parton showering and hadronization, and PGS [60] as a fast detector simulation. Combining the ATLAS lepton triggers and off-line cuts from [57], we select opposite sign dilepton events satisfying any of the following requirements: a muon pair with $p_T > 15$ GeV for the leading muon and $p_T > 10$ GeV for the subleading one, an electron pair with both $p_T > 15$ GeV, or an electron and a muon with p_T above 15 and 10 GeV, respectively. Electrons (muons) are accepted only if their pseudorapidity is $|\eta| < 2.47$ (2.5). We require the invariant mass of the lepton pair to be $30 \text{ GeV} < m_{l\bar{l}} < 100 \text{ GeV}$ for $e\mu$ pairs, or $30 \text{ GeV} < m_{l\bar{l}} < 75 \text{ GeV}$ for same flavor pairs. The missing p_T is required to be above 20 (40) GeV for $e\mu$ events (ee or $\mu\mu$ events). The azimuthal separation between the two leptons is required to be $0.5 < \Delta\phi_{ll} < 2.5$.

Additional cuts are placed with the goal of enriching the event sample in VBF events: at least two jets with p_T above 40 GeV for the leading jet and above 25 GeV for the subleading jet are required, with the rapidity difference between the two leading jets above $|\Delta\eta| > 3$ and the invariant mass $m_{jj} > 350 \text{ GeV}$. We veto events with an additional jet with $p_T > 25 \text{ GeV}$ and $|\eta| < 2.4$ in the pseudorapidity region between the two leading jets.

The reconstructed invariant mass is calculated using the collinear approximation in which all invisible particles are assumed to be collinear with either of the two leptons. The fractions of the parent τ 's momenta carried by the charged leptons are denoted by x_1 and x_2 . To be able to compare with ATLAS data from the $h \rightarrow \tau\tau$ search, we compute x_1 and x_2 assuming *two* neutrinos in the final state, even though $h \rightarrow \tau\mu$ yields only one. x_1 and x_2 are then obtained as the solutions of the transverse momentum equation $\mathbf{p}_{miss,T} = (1 - x_1)\mathbf{p}_{1,T} + (1 - x_2)\mathbf{p}_{2,T}$, where $\mathbf{p}_{1,2,T}$ are the transverse momenta of the charged leptons. Following [57], we require $0.1 < x_{1,2} < 1$, which removes less than a per cent of $h \rightarrow \tau\tau$ events, but nearly 60% of our $h \rightarrow \tau\mu$ events. Thus, relaxing this cut would enhance the sensitivity to $h \rightarrow \tau\mu$

⁴ In fact, it may be interesting to apply the collinear approximation more often in resonance searches. A search for a collinear mass resonance can be sensitive to any particle which decays to boosted objects whose further decay may introduce missing energy.

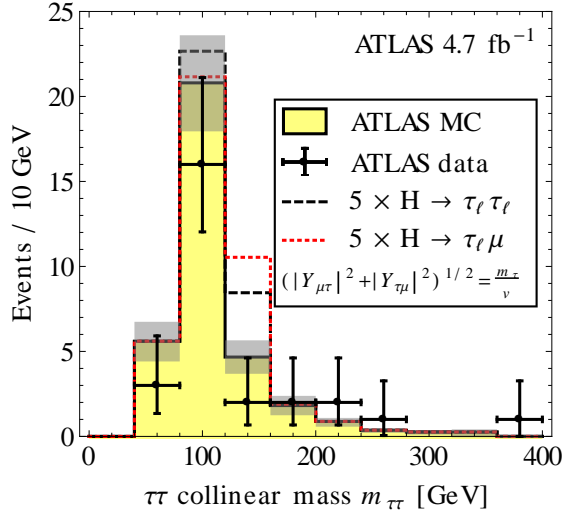


Figure 9: Background rates and $h \rightarrow \tau\mu$, $h \rightarrow \tau\tau$ signal rates in the ATLAS search for fully leptonic $h \rightarrow \tau\tau$ decays, optimized for Higgs production in vector boson fusion. The backgrounds expected by ATLAS [57] are shown in yellow, with grey bands for the systematic uncertainty. Our estimates for the $\tau\mu$ signal at $\sqrt{Y_{\tau\mu}^2 + Y_{\mu\tau}^2} = m_\tau/v$ (red) and the SM $h \rightarrow \tau\tau$ signal (black), which we include for reference, are scaled by a factor 5 for illustrative purposes only.

decays so long as it does not introduce large backgrounds. Nonetheless, we are still able to use the current search for $h \rightarrow \tau\tau$ to produce an interesting bound on $\text{BR}(h \rightarrow \tau\mu)$.

In Fig. 9 we show the background distribution for the collinear mass along with the expected shape of a LFV $h \rightarrow \tau\mu$ signals (scaled by a factor five for illustrative purposes only), and we compare to the observed data. The background expectation is taken from [57]. The backgrounds and the data in Fig. 9 include events for all three combinations of lepton flavor (even though our $\tau\mu$ signal does not induce ee events) because only this information is available from ATLAS. For validation purposes, we have also simulated SM $h \rightarrow \tau\tau$ events, and comparing the rate and shape to Ref. [57] we find agreement to within 20%.

The $\tau\mu$ signal is predominantly concentrated in the 120–160 GeV bin, so that the expected and observed limits on the flavor violating Yukawa couplings can be derived from a simple single-bin analysis. If we denote the number of expected background events by $B = 4.7$, the number of expected signal events for a given set of Yukawa couplings by S , and the number of observed events by $O = 2$, the expected (observed) one-sided 95% C.L. frequentist limit on S is defined by the requirement that the probability to observe $\leq B$ ($\leq O$) events is

95% C.L. limit	$\text{BR}(h \rightarrow \tau\mu)$	$\sqrt{Y_{\tau\mu}^2 + Y_{\mu\tau}^2}$	$\text{BR}(h \rightarrow \tau e)$	$\sqrt{Y_{\tau e}^2 + Y_{e\tau}^2}$
expected	28%	0.018	27%	0.017
observed	13%	0.011	13%	0.011

Table III: Expected and observed 95% C.L. limits on the $h \rightarrow \tau\mu$ and $h \rightarrow \tau e$ branching ratios, as well as limits on the corresponding Yukawa couplings. The limits are derived by assuming the SM Higgs production rates and recasting the search for SM $h \rightarrow \tau\tau \rightarrow 2\ell + 2\nu$ decays in the VBF channel from [57].

5%. The relevant probability distribution of the data here is a Poisson distribution with mean $B + S$. We can also include the systematic uncertainty in the 120–160 GeV bin, which is $\Delta_{\text{sys}} \simeq \pm 0.99$, in a conservative way by instead using a Poisson distribution with mean $B + S - \Delta_{\text{sys}}$. Assuming the Higgs is produced with the Standard Model rates, this procedure leads to the bound on $\text{BR}(h \rightarrow \tau\mu)$ and the analogous bound on $\text{BR}(h \rightarrow \tau e)$ shown in Table III (see also Figure 6).

B. Comparison of $h \rightarrow \tau\mu$ to $h \rightarrow \tau\tau$

We now discuss the experimental differences and similarities between $h \rightarrow \tau\tau$ and $h \rightarrow \tau\mu$ decays to determine an optimized search strategy for the latter. We focus here on $h \rightarrow \tau_{\text{had}}\tau_{\mu}$, where τ_{μ} denotes a τ that decays into a muon and two neutrinos and τ_{had} denotes a τ decaying hadronically. This channel is actively searched for, both at ATLAS [57] and at CMS [27], and is the most sensitive channel in the CMS $h \rightarrow \tau\tau$ search. (In ATLAS, fully leptonic τ events provide similar sensitivity to semi-hadronic ones.) It will also be the channel that we will devise a dedicated search for in the next subsection.

There are a few notable differences between the $h \rightarrow \tau_{\text{had}}\tau_{\mu}$ and $h \rightarrow \tau_{\text{had}}\mu$ decay channels:

- *Branching Ratios.* The branching fraction for $h \rightarrow \tau_{\text{had}}\tau_{\mu}$ is $2 \times \text{BR}(h \rightarrow \tau\tau) \times \text{BR}(\tau \rightarrow \text{had}) \times \text{BR}(\tau \rightarrow \mu)$, whereas for $h \rightarrow \tau_{\text{had}}\mu$ it is simply $\text{BR}(h \rightarrow \tau\mu) \times \text{BR}(\tau \rightarrow \text{had})$. For $(Y_{\tau\mu}^2 + Y_{\mu\tau}^2)^{1/2} \sim Y_{\tau\tau}$ the signal for $h \rightarrow \tau_{\text{had}}\mu$ is thus a factor of ~ 2.9 larger.
- *Lepton Flavor.* The flavor violating decays can lead to different rates for muons and electrons in the final state, whereas $\tau\tau$ decays lead to equal μ and e rates. Thus, if the

various lepton flavor combinations were studied separately in the $h \rightarrow \tau\tau$ analyses, stronger bounds on flavor violating decays could be inferred.

- *Kinematics and Efficiencies.* In $h \rightarrow \tau_{\text{had}}\tau_{\mu}$ decays the muon carries an average energy $\sim m_h/6$, while for $h \rightarrow \tau_{\text{had}}\mu$ it carries $\sim m_h/2$. Furthermore, in $h \rightarrow \tau_{\text{had}}\mu$ events the missing energy is roughly aligned with the hadronic τ . As a result the two channels can have different efficiencies given the same cuts. For example, in the VBF analysis described below (mimicking [27]) the efficiency for $h \rightarrow \tau_{\text{had}}\tau_{\mu}$ is a factor of ~ 1.8 lower than for $h \rightarrow \tau_{\text{had}}\mu$ events, mostly because many of the muons in the $h \rightarrow \tau_{\text{had}}\tau_{\mu}$ sample fall below the $p_T < 17$ GeV cut.
- *Mass reconstruction.* The LHC collaborations use highly optimized procedures for reconstructing the $\tau_{\text{had}}\tau_{\mu}$ invariant mass. ATLAS uses the Missing Mass Calculator (MMC) from [58], while CMS uses an in-house maximum likelihood analysis [27]. These procedures use $\mathbf{p}_{\text{miss},T}$ and the 3-momenta of the muon and the τ jet as input and estimate the neutrino momenta by assuming typical τ decay kinematics. For $h \rightarrow \tau\tau$ events, the MMC procedure returns an invariant mass with high efficiency ($\sim 97\%$) and gives a Higgs mass resolution of $\sim 20\%$. If the event is not from $h \rightarrow \tau\tau$ but instead from $h \rightarrow \tau_{\text{had}}\mu$, then i) the efficiency will be significantly lower since the kinematics can be completely inconsistent with a $\tau\tau$ event, and ii) the reconstructed Higgs mass will be significantly higher as the MMC will assume that the hard muon is accompanied by two roughly collinear and hard neutrinos. This illustrates that a mass reconstruction procedure designed for the specific final state under consideration is mandatory to obtain the best possible sensitivity.
- *Backgrounds.* The backgrounds for $h \rightarrow \tau_{\text{had}}\tau_{\mu}$ and $h \rightarrow \tau_{\text{had}}\mu$ events are similar, but because of the different invariant mass reconstruction techniques, the reconstructed background spectra will typically be harder for a $h \rightarrow \tau_{\text{had}}\tau_{\mu}$ analysis, which assumes three neutrinos in the final state, than for a $h \rightarrow \tau_{\text{had}}\mu$ analysis which assumes only one. This implies, for instance, that the peak from the $Z \rightarrow \tau\tau$ background will appear at a $\tau_{\text{had}}\tau_{\mu}$ invariant mass around 90 GeV in a search for $h \rightarrow \tau_{\text{had}}\tau_{\mu}$, but well below (and thus further away from the signal peak) in a dedicated $h \rightarrow \tau_{\text{had}}\mu$ analysis.

These considerations show that the LHC is potentially more sensitive to flavor violating

$h \rightarrow \tau_{\text{had}}\mu$ decays than to the SM $h \rightarrow \tau\tau$ channel. We now discuss a possible strategy for a tailored $h \rightarrow \tau_{\text{had}}\mu$ analysis.

C. A dedicated $h \rightarrow \tau\mu$ analysis

We now investigate the potential of a dedicated $h \rightarrow \tau_{\text{had}}\mu$ analysis which follows closely the CMS search for $h \rightarrow \tau_{\text{had}}\tau_{\mu}$ [27].⁵ The most important difference to that analysis will be a different algorithm for reconstructing the $\tau\mu$ invariant mass. In particular, since the $\tau_{\text{had}}\mu$ final state contains only one neutrino (from the hadronic τ), this mass reconstruction can always be done exactly (i.e. the neutrino momentum can be determined) up to a two-fold ambiguity.

An important background for $h \rightarrow \tau\mu$ is $Z + \text{jets}$, where either the Z decays into $\tau^+\tau^-$ and one of the τ 's decays further into a muon, or the Z decays into $\mu^+\mu^-$ and one of the jets fakes a τ . Another important background is $W + \text{jets}$, followed by $W \rightarrow \mu\nu_{\mu}$ and a jet faking a τ . We neglect the small $t\bar{t}$ background, where a final state τ can come from a W decay or be faked by a jet, and a muon can originate from a W decay or from a leptonic τ decay. We also do not consider backgrounds from QCD multijet production because making reliable predictions for these events requires full detector simulations. Based on the CMS $h \rightarrow \tau_{\mu}\tau_{\text{had}}$ search [27] we expect them to be about as large as the $W + \text{jets}$ background in the invariant mass region around 125 GeV.

To simulate the parton-level signal and background events, we use MadGraph 5 v1.4.6 [59], with an extended version of the Higgs Effective Theory model to include flavor-violating Higgs interactions. We use Pythia 6.4 for parton showering and hadronization and Delphes 2.0.2 [62] as a fast detector simulation. We have compared the τ detection efficiency as well as the fake rate from QCD jets in Delphes 2.0.2 to the corresponding performance indicators of several CMS τ tagging algorithm. With a tagging efficiency of ~ 0.2 and a fake rate between 0.2% at low p_T and 1% at $p_T \gtrsim 60$ GeV, Delphes somewhat underestimates the performance of the CMS τ tagging algorithms [63]. (We have also studied τ tagging in PGS [60], but found it to be even farther away from what CMS can achieve.) To compensate for the imperfections in our treatment of τ -tagging, and for other inaccuracies in

⁵ For semileptonically decaying τ , search strategies similar to the ones investigated in Ref. [61] for flavor violating $Z \rightarrow \tau\mu$ decays could be used.

our simulations, we normalize our background distributions to the expected event numbers from [27], Table 2. We also normalize the $h \rightarrow \tau\mu$ signal using the same scaling factor as for the SM $h \rightarrow \tau_{\text{had}}\tau\mu$ events.

In the analysis we require exactly one muon with $p_T > 17$ GeV and $|\eta| < 2.1$ in the final state and exactly one jet tagged as a hadronic τ decay with $p_T > 20$ GeV and $|\eta| < 2.3$. The muon and the τ are required to have opposite charge. In [27], it was found that the best signal-to-background ratio is achieved in the events where the Higgs boson was produced through vector boson fusion (VBF), and we confirm this in our own simulations. To enrich the data sample in VBF events, we consider only events with a pair of jets j_1, j_2 satisfying $|\Delta\eta| > 4.0$, $\eta_1\eta_2 < 0$, $m_{jj} > 400$ GeV and no other jets with $p_T > 30$ GeV in the pseudorapidity region between the j_1 and j_2 . Here, $\Delta\eta = \eta_1 - \eta_2$ is the pseudorapidity difference between the two jets and m_{jj} is the invariant mass of the jet pair. Non- τ jets are included in the analysis so long as their p_T is above 30 GeV and their pseudorapidity is $|\eta| < 4.7$. In the CMS analysis [27], the transverse mass of the muon and the missing energy is restricted to be below 40 GeV in order to suppress the $W + \text{jets}$ background. This works because in $W + \text{jets}$ events, the muon and the neutrino from $W \rightarrow \mu\nu_\mu$ tend to be more back-to-back than in $h \rightarrow \tau_\mu\tau_{\text{had}}$, where both τ 's contribute to the missing energy. In $h \rightarrow \tau_{\text{had}}\mu$, however, the muon and the missing energy also tend to be back-to-back, so that the $m_T(\mu, \mathbf{p}_{\text{miss},T})$ cut also removes a large fraction of signal events.

In light of this we show in Fig. 10 the expected signal and background rates for $h \rightarrow \tau\mu$ as a function of the μ - τ invariant mass $m_{\tau\mu}$ both with and without the transverse mass cut. In computing $m_{\tau\mu}$ for each event, we have used energy and momentum conservation to compute the z -component of the neutrino momentum $p_{\nu,z}$. There are two solutions to these equations, and we arbitrarily pick the smaller of the two. (We have checked that choosing the larger value for $p_{\nu,z}$ yields a very similar plot. This is related to the fact that $m_\tau \ll m_h$, so that the τ 's decay products are almost collinear.) As shown in the right panel of Fig. 10, dropping the transverse mass cut increases the W plus jets background, but has the benefit of retaining more signal. The transverse mass distributions for signal and background is shown in Fig. 11. Assuming the W plus jets and QCD backgrounds can be controlled reasonably, relaxing this cut may be worthwhile.

In summary, Fig. 10 shows that for flavor violating Yukawa couplings well allowed by low energy precision measurements, a spectacular signal can be expected in a dedicated search

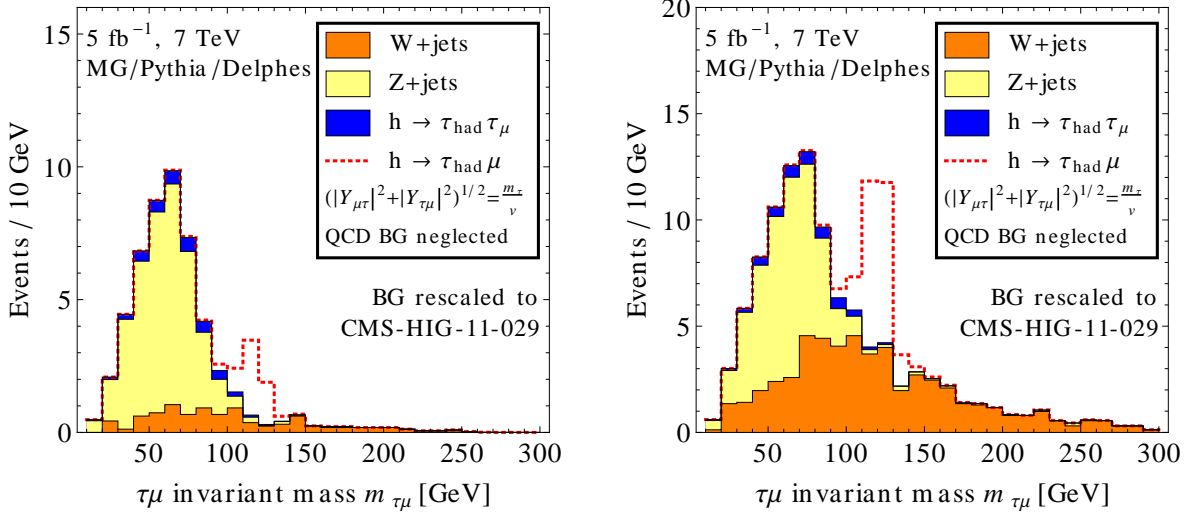


Figure 10: Signal and background rates for $h \rightarrow \tau\mu$ events in a CMS-like search (see text) as a function of the reconstructed μ - τ invariant mass $m_{\tau\mu}$ for a vector boson fusion-enriched event sample. In the left panel the transverse mass cut $m_T(\mu, \mathbf{p}_{\text{miss},T}) < 40$ GeV is included, while in the right panel it is omitted. The QCD multijet background and the small $t\bar{t}$ background, are not included. The value chosen for $\sqrt{Y_{\tau\mu}^2 + Y_{\mu\tau}^2}$ is well within the region allowed by other searches for flavor violation in the μ - τ system (see Sec. III).

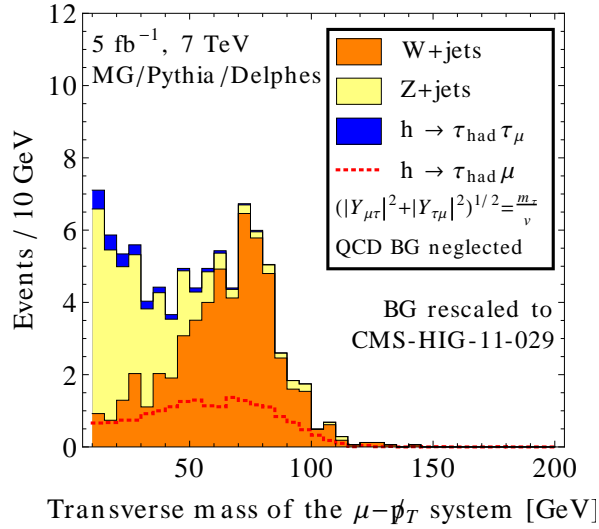


Figure 11: The transverse mass distribution of the muon-missing energy system for the backgrounds and for the $\tau_{\text{had}}\mu$ signal.

at the LHC. Such a search would cut deeply into the allowed parameter space of the flavor violation Higgs to $\tau\mu$ couplings.

VI. CONCLUSIONS

The LHC experiments have recently discovered a Higgs-like resonance with a mass around 125 GeV. In this paper we have examined the constraints on potential flavor violating couplings of this resonance, assuming it is indeed a scalar boson. In deriving the constraints we have assumed that that flavor changing neutral currents are dominated by the Higgs contributions, which may be thought of as a “simplified model” approach to flavor violation in light of the Higgs discovery. (In a complete model, cancellations between Higgs-induced flavor violation and flavor violation induced by other new physics is possible, but we do not pursue this possibility here.)

We have refined the indirect constraints on the flavor violating Yukawa couplings Y_{ij} using results from rare decay searches, magnetic and electric dipole moment measurement, and the LHC. All constraints are summarized in Tables I and II and in Figs. 6 and 8. We have compared the bounds to the loose naturalness criterion that the off-diagonal Yukawa couplings are not much bigger than the geometric mean of diagonal terms, $Y_{ij} \lesssim \sqrt{Y_{ii}Y_{jj}}$, and we have discussed to what extent the LHC can probe flavor violating decays of the form $h \rightarrow \bar{f}_i f_j$ (or in the case of flavor violating top–Higgs couplings the decay $t \rightarrow h f_i$).

We draw the following conclusions:

Natural Flavor Violation. The existing constraints involving only the first two generations of fermions, quarks or leptons, are strong enough that natural FV is already being probed by meson oscillations, $\mu \rightarrow e$ conversion and $\mu \rightarrow e\gamma$. This conclusion also holds for FV couplings to b quarks. In contrast, the FV couplings involving τ leptons or top quarks are allowed to have natural size (unless there is a large hierarchy between Y_{ij} and Y_{ji}). This means that they are potentially observable, either at the LHC or in future low energy experiments.

Opportunities for the LHC. The LHC has an opportunity to probe a large part of the allowed parameter space for $h \rightarrow \tau\mu$ and $h \rightarrow \tau e$ couplings. An LHC search in these channels would be very similar to the existing searches for $h \rightarrow \tau\tau$, and recasting the latter already gives the best bounds on the flavor violating Yukawa couplings $Y_{\tau e}$, $Y_{e\tau}$, $Y_{\tau\mu}$, and

$Y_{\mu\tau}$ already now. A dedicated LHC search could improve the limits significantly. The reason why Higgs decays are very constraining is that the SM width of a 125 GeV Higgs boson is very small, $\Gamma_h \simeq 4$ MeV [47], so that the flavor violating couplings of the Higgs can have a significant effect. Another illustration of the LHC’s discovery potential for flavor violating Higgs couplings is that even the global fits of potential deviations in the dominant SM Higgs decay modes, $h \rightarrow WW, ZZ, b\bar{b}, \tau\tau, \gamma\gamma$, already give meaningful bounds on the FV Higgs decays. The results from these global fits are usually presented as bounds on the invisible decay width of the Higgs, but these bounds applies equally well to the sum of all the modes that have not been included in the fits. The constraint $\text{BR}(h \rightarrow \text{invisible}) \lesssim \mathcal{O}(70\%)$ (at 95 % CL, with modest theory assumptions [48, 64–66]) is comparable to the constraints on $\text{BR}(h \rightarrow \tau\mu)$ and $\text{BR}(h \rightarrow \tau e)$ from precision searches of FCNCs in the lepton sector.

Finally, flavor violating Higgs couplings involving the top quark are poorly constrained, and in fact, the LHC already provides the strongest limits on such couplings, see Fig. 8 and Section IV.

Acknowledgments

We thank Edward Boos, Alejandro Celis, Andreas Crivellin, Zackaria Chacko, Ricky Fok, Graham Kribs, Uli Haisch, Ethan Neil, Takemichi Okui, André Schöning and Ze’ev Surujon for valuable discussions, and LOT Polish Airlines for free internet access during a crucial phase of this project. This material is based upon work supported in part by the National Science Foundation under Grant No. PHYS-1066293 and the hospitality of the Aspen Center for Physics. JZ was supported in part by the U.S. National Science Foundation under CAREER Grant PHY1151392. Fermilab is operated by Fermi Research Alliance under contract DE-AC02-07CH11359 with the United States Department of Energy.

Appendix A: Further details on leptonic FCNCs

In this appendix we collect detailed expressions for the FCNC processes $\tau \rightarrow \mu\gamma$ and $\mu \rightarrow e$ conversion in nuclei.

1. One loop expressions for $\tau \rightarrow \mu\gamma$, $\tau \rightarrow e\gamma$, $\mu \rightarrow e\gamma$

The $\tau \rightarrow \mu\gamma$ effective Lagrangian is given in Eq. (11). The Wilson coefficients $c_{L,R}$ are given by

$$c_L = F(m_\tau, m_\tau, m_\mu, m_h, 0, Y) + F(m_\tau, m_\mu, m_\mu, m_h, 0, Y), \quad (\text{A1})$$

$$c_R = F(m_\tau, m_\tau, m_\mu, m_h, 0, Y^\dagger) + F(m_\tau, m_\mu, m_\mu, m_h, 0, Y^\dagger), \quad (\text{A2})$$

with the loop functions

$$F(m_i, m_f, m_j, m_h, q^2, Y) = \frac{1}{4m_i} \int_0^1 dx dy dz \delta(1-x-y-z) \frac{xz m_j Y_{jf} Y_{if}^* + yz m_i Y_{fj}^* Y_{fi} + (x+y)m_f Y_{fj}^* Y_{if}^*}{zm_h^2 - xz m_j^2 - yz m_i^2 + (x+y)m_f^2 - xyq^2}. \quad (\text{A3})$$

Here m_μ , m_τ and m_h are the muon, tau and Higgs masses, respectively, q is the 4-momentum of the photon, and Y is the Yukawa coupling matrix. Note that c_L and c_R differ only by the replacement $Y_{ij} \leftrightarrow Y_{ji}^*$. The first terms in Eqs. (A1) and (A2) arise from the first diagram in Fig. 1 (with a τ propagating in the loop), whereas the second terms arise from the second diagram (with a μ in the loop). Expanding in powers of m_μ/m_τ and m_τ/m_h and keeping only the leading terms (so that only the first terms in (A1), (A2) contribute), the above expressions simplify to (13) if the diagonal Yukawa couplings are real. The simplified expressions for $\tau \rightarrow e\gamma$ and $\mu \rightarrow e\gamma$ (with a muon running in the loop) are obtained from (13) with trivial modifications, while the simplified expression for $\mu \rightarrow e\gamma$ with a τ running in the loop is given in Eq. (16).

2. Two loop expressions for $\tau \rightarrow \mu\gamma$, $\tau \rightarrow e\gamma$ and $\mu \rightarrow e\gamma$

At two loops there are numerically important diagrams with top or W running in the loop, attached to the Higgs. Here we translate the results of [36] into our notation and adapt them to the case of $\tau \rightarrow \mu\gamma$. The diagrams with top and photon in the loops (see Fig. 12 top left) contributes as

$$\Delta c_L^{t\gamma} = -6\kappa Q_t^2 \frac{v}{m_t} Y_{\tau\mu}^* [\text{Re}(Y_{tt})f(z_{th}) - i\text{Im}(Y_{tt})g(z_{th})], \quad (\text{A4})$$

while the W -photon 2-loop contribution is

$$\Delta c_L^{W\gamma} = \kappa Y_{\tau\mu}^* \left[3f(z_{Wh}) + 5g(z_{Wh}) + \frac{3}{4}g(z_{Wh}) + \frac{3}{4}h(z_{Wh}) + \frac{f(z_{Wh}) - g(z_{wh})}{2z_{Wh}} \right]. \quad (\text{A5})$$

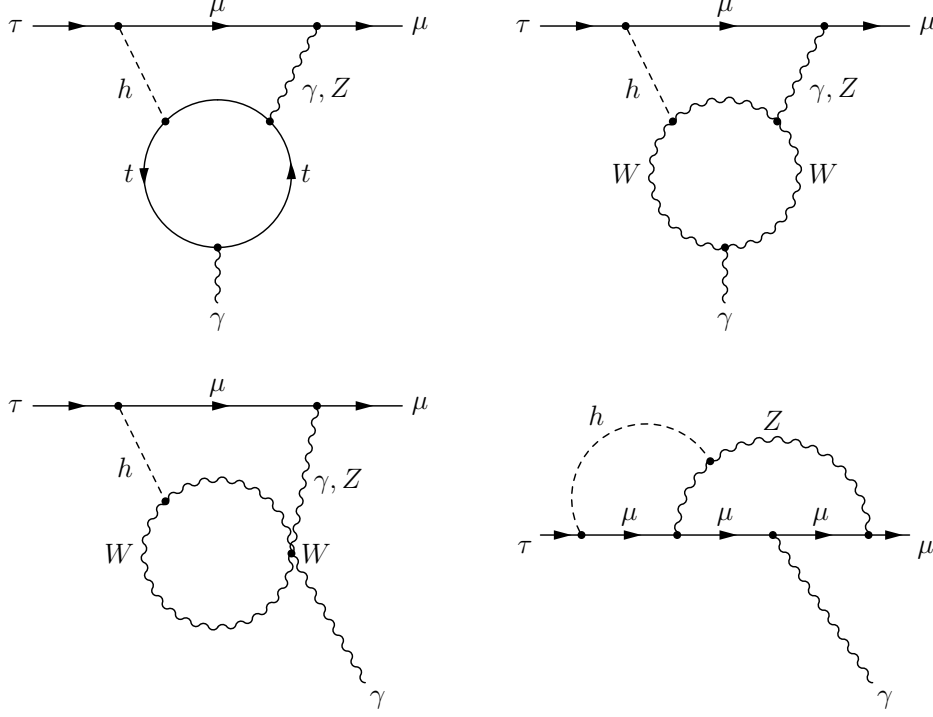


Figure 12: The two loop diagrams contributing to $\tau \rightarrow \mu\gamma$.

Here we have already added the contributions from the would-be Goldstone bosons that get eaten by the W . The contributions to Δc_R^i are obtained from the above by replacing $Y_{\tau\mu}^* \rightarrow Y_{\mu\tau}$ and $Y_{tt} \rightarrow Y_{tt}^*$. The loop functions are

$$f(z) = \frac{1}{2}z \int_0^1 dx \frac{1-2x(1-x)}{x(1-x)-z} \log \frac{x(1-x)}{z}, \quad (\text{A6})$$

$$g(z) = \frac{1}{2}z \int_0^1 dx \frac{1}{x(1-x)-z} \log \frac{x(1-x)}{z}, \quad (\text{A7})$$

$$h(z) = z^2 \frac{\partial}{\partial z} \left(\frac{g(z)}{z} \right) = \frac{z}{2} \int_0^1 \frac{dx}{z-x(1-x)} \left[1 + \frac{z}{z-x(1-x)} \log \frac{x(1-x)}{z} \right], \quad (\text{A8})$$

the arguments are $z_{th} = m_t^2/m_H^2$, $z_{Wh} = m_W^2/m_H^2$, while the prefactor is

$$\kappa = \frac{\alpha}{16\pi} \frac{g^2}{m_W^2} \frac{v}{m_\tau} = \frac{\alpha}{2\sqrt{2}\pi} G_F \frac{v}{m_\tau}. \quad (\text{A9})$$

The contributions from the 2-loop diagrams with an internal Z are smaller as they are suppressed by $1-4s_W^2 \simeq 0.08$. They are

$$\begin{aligned} \Delta c_L^{tZ} &= -6\kappa Q_t \frac{(1-4s_W^2)(1-4Q_t s_W^2)}{16s_W^2 c_W^2} \frac{v}{m_t} Y_{\tau\mu}^* \times \\ &\times [\text{Re}(Y_{tt})\tilde{f}(z_{th}, z_{tZ}) - i\text{Im}(Y_{tt})\tilde{g}(z_{th}, z_{tZ})], \end{aligned} \quad (\text{A10})$$

$$\begin{aligned} \Delta c_L^{WZ} = & \kappa \frac{1 - 4s_W^2}{4s_W^2} Y_{\tau\mu}^* \left\{ \frac{1}{2}(5 - t_W^2) \tilde{f}(z_{th}, z_{WZ}) + \frac{1}{2}(7 - 3t_W^2) \tilde{g}(z_{th}, z_{WZ}) \right. \\ & \left. + \frac{3}{4}g(z_{th}) + \frac{3}{4}h(z_{th}) + \frac{1}{4z_{th}}(1 - t_W^2) [\tilde{f}(z_{th}, z_{WZ}) - \tilde{g}(z_{th}, z_{WZ})] \right\}, \end{aligned} \quad (\text{A11})$$

with $s_W \equiv \sin \theta_W$, $c_W \equiv \cos \theta_W$, $t_W \equiv \tan \theta_W$, $z_{tz} \equiv m_t^2/m_Z^2$, $z_{WZ} \equiv m_W^2/m_Z^2$ and the loop functions

$$\tilde{f}(x, y) = \frac{yf(x)}{y-x} + \frac{xf(y)}{x-y}, \quad \tilde{g}(x, y) = \frac{yg(x)}{y-x} + \frac{xg(y)}{x-y}. \quad (\text{A12})$$

The Δc_R^i are obtained by replacing $Y_{\mu e}^* \rightarrow Y_{e\mu}$ and $Y_{tt} \rightarrow Y_{tt}^*$ in the above expressions. In addition there are also contributions called ‘‘set C’’ in [36]. An example for one of these diagrams is the last diagram in Fig. 12. Since the expressions for these diagrams are long we do not write them out explicitly. The ‘‘set C’’ contribution to Δc_L is obtained from [36] by multiplying their Eq. (20) by $-\kappa$ and replacing $\sum_a \cos \varphi_a \Delta_{e\mu}^a \rightarrow Y_{\tau\mu}^*$.

The $\tau \rightarrow e\gamma$ expressions are obtained by replacing $Y_{\tau\mu} \rightarrow Y_{\tau e}$ and $Y_{\mu\tau} \rightarrow Y_{e\tau}$ in the above expressions, while for $\mu \rightarrow e\gamma$ the replacements are $Y_{\tau\mu} \rightarrow Y_{\mu e}$, $Y_{\mu\tau} \rightarrow Y_{e\mu}$ and $m_\tau \rightarrow m_\mu$.

3. Details on $\mu \rightarrow e$ conversion bounds

The most general effective Lagrangian for $\mu \rightarrow e$ conversion in nuclei is [67]

$$\begin{aligned} \mathcal{L} = & c_L \frac{e}{8\pi^2} m_\mu (\bar{e} \sigma^{\alpha\beta} P_L \mu) F_{\alpha\beta} - \frac{1}{2} \sum_q \left[g_{LS}^q (\bar{e} P_R \mu) (\bar{q} q) + g_{LP}^q (\bar{e} P_R \mu) (\bar{q} \gamma_5 q) \right. \\ & \left. + g_{LV}^q (\bar{e} \gamma^\mu P_L \mu) (\bar{q} \gamma_\mu q) + g_{LA}^q (\bar{e} \gamma^\mu P_L \mu) (\bar{q} \gamma_\mu \gamma_5 q) + \frac{1}{2} g_{LT}^q (\bar{e} \sigma^{\alpha\beta} P_R \mu) (\bar{q} \sigma_{\alpha\beta} q) \right] + L \leftrightarrow R. \end{aligned} \quad (\text{A13})$$

The Wilson coefficients c_L and c_R of the magnetic dipole operator are the same as the ones introduced for $\mu \rightarrow e\gamma$ in Appendix A 2, with the replacements $\tau \rightarrow \mu$, $\mu \rightarrow e$. They receive contributions from one-loop and two-loop diagrams, with the two-loop diagrams being orders of magnitude larger numerically.

The scalar operators in Eq. (A13), generated by the first diagram in Fig. 5, are given by

$$g_{LS}^q = -\frac{2}{m_h^2} Y_{e\mu} \text{Re}(Y_{qq}), \quad g_{RS}^q = -\frac{2}{m_h^2} Y_{\mu e}^* \text{Re}(Y_{qq}). \quad (\text{A14})$$

The vector operators are determined at one-loop by the last two diagrams in Fig. 5, with either a muon or an electron running in the loop. Explicitly, we find (with $\tilde{g}_{LV}^{(p)} = 2g_{LV}^u + g_{LV}^d$)

and $\tilde{g}_{LV}^{(n)} = 2g_{LV}^d + g_{LV}^u$)

$$\begin{aligned} \tilde{g}_{LV}^{(p)} = g_{LV}^q/Q_q = & -\frac{\alpha}{2\pi q^2} [G(m_\mu, m_\mu, m_e, m_h, q^2, Y) - G(m_\mu, m_\mu, m_e, m_h, 0, Y) \\ & + G(m_\mu, m_e, m_e, m_h, q^2, Y) - G(m_\mu, m_e, m_e, m_h, 0, Y)]. \end{aligned} \quad (\text{A15})$$

Here, Q_q is the charge of quark q , and $\tilde{g}_{RV}^{(p)}$, g_{RV}^q is given by Eq. (A15) with the replacement $Y \rightarrow Y^\dagger$. The loop function in (A15) is

$$\begin{aligned} G(m_i, m_f, m_j, m_h, q^2, Y) = & \int_0^1 dx \int_0^{1-x} dy \left[Y_{jf} Y_{if}^* \log \Delta - \frac{1}{\Delta} m_i m_j z^2 Y_{jf}^* Y_{fi} \right. \\ & \left. - \frac{1}{\Delta} (m_f m_j z Y_{jf}^* Y_{if}^* + m_f m_i z Y_{jf} Y_{fi} + [q^2 xy + m_f^2] Y_{jf} Y_{if}^*) \right], \end{aligned} \quad (\text{A16})$$

where we have defined $\Delta \equiv zm_h^2 - xzm_j^2 - yzm_i^2 + (x+y)m_f^2 - xyq^2$ and $z = 1 - x - y$. Note that we subtract the value of the one-loop vertex correction at $q^2 = 0$, which gets absorbed into the wave function and mass renormalizations. g_{LV}^q and g_{RV}^q also receive two-loop contributions from diagrams similar to the ones relevant for c_L , c_R (see Fig. 12). To the best of our knowledge, analytic expressions for these contributions are not available in the literature, and are thus not included in our numerical results. While the one-loop vector contributions are smaller than the one-loop dipole ones in the $\mu \rightarrow e$ conversion rate, and can be neglected, it would be desirable to also evaluate the two-loop vector terms in order to verify that all numerically important contributions have been taken into account.

All other Wilson coefficients in Eq. (A13) are zero, $g_{LP}^q = g_{RP}^q = g_{LA}^q = g_{RA}^q = g_{LT}^q = g_{RT}^q = 0$.

When computing the $\mu \rightarrow e$ conversion rate in nuclei care must be taken to account for the nuclear matrix elements $\langle N|\bar{q}q|N\rangle$, $\langle N|\bar{q}\gamma^\mu q|N\rangle$ and $\langle N|F^{\mu\nu}|N\rangle$ and for the overlap of the initial muon wave function and the final state electron wave function. We follow [67] and obtain

$$\begin{aligned} \Gamma(\mu \rightarrow e \text{ conversion}) = & \left| -\frac{e}{16\pi^2} c_R D + \tilde{g}_{LS}^{(p)} S^{(p)} + \tilde{g}_{LS}^{(n)} S^{(n)} + \tilde{g}_{LV}^{(p)} V^{(p)} \right|^2 \\ & + \left| -\frac{e}{16\pi^2} c_L D + \tilde{g}_{RS}^{(p)} S^{(p)} + \tilde{g}_{RS}^{(n)} S^{(n)} + \tilde{g}_{RV}^{(p)} V^{(p)} \right|^2. \end{aligned} \quad (\text{A17})$$

The electromagnetic penguin and vector contributions were already given above. Note that vector couplings to neutrons are absent due to the neutron's vanishing electric charge. The scalar coefficients for proton and neutron coupling are given in terms of the quark level

coefficients by

$$\tilde{g}_{LS,RS}^{(p)} = \sum_q g_{LS,RS}^q \frac{m_p}{m_q} f^{(q,p)}, \quad \tilde{g}_{LS,RS}^{(n)} = \sum_q g_{LS,RS}^q \frac{m_n}{m_q} f^{(q,n)}. \quad (\text{A18})$$

Here, the sum runs over all quark flavors, $q = u, d, s, c, b, t$.

The nucleon matrix elements $f^{(q,p)} \equiv \langle p | m_q \bar{q} q | p \rangle / m_p$ are calculated according to [68], but using an updated value for the nucleon sigma term $\Sigma_{\pi N} = 55$ MeV [69] (If the value of the nucleon sigma term is even smaller, as indicated by recent unquenched lattice results, our bounds would become weaker). The nucleon matrix elements are numerically

$$f^{(u,p)} = f^{(d,n)} = 0.024, \quad f^{(d,p)} = f^{(u,n)} = 0.033, \quad f^{(s,p)} = f^{(s,n)} = 0.25, \quad (\text{A19})$$

while the contributions from the heavier quarks are

$$f^{(c,p)} = f^{(b,p)} = f^{(t,p)} = \frac{2}{27} \left(1 - \sum_{q=u,d,s} f^{(q,p)} \right). \quad (\text{A20})$$

with the same values for neutrons. In the above expressions, m_q denotes a quark mass, m_p is the proton mass, and m_n is the neutron mass. The coefficients D , $V^{(p)}$, $S^{(p)}$, and $S^{(n)}$ are overlap integrals of the muon, electron and nuclear wave function. They are tabulated for various target materials in [67]. The best limits are obtained from bounds on $\mu \rightarrow e$ conversion on gold, $\Gamma(\mu \rightarrow e)_{\text{Au}} / \Gamma_{\text{capture Au}} < 7 \times 10^{-13}$ (90% CL) [70], for which in units of $m_\mu^{5/2}$ the overlap integrals are $D = 0.189$, $S^{(p)} = 0.0614$, $V^{(p)} = 0.0974$, $S^{(n)} = 0.0918$, using the same distributions for neutrons and protons in the nucleus. For the SM capture rate, we use a value $\Gamma_{\text{capture Au}} = 13.07 \times 10^6 \text{ s}^{-1}$ in the calculation [67].

-
- [1] The ATLAS collaboration (2012), ATLAS-CONF-2012-093, available from <http://cdsweb.cern.ch/record/1460439/files/ATLAS-CONF-2012-093.pdf>.
 - [2] The CMS collaboration (2012), CMS-PAS-HIG-12-020, available from <http://cdsweb.cern.ch/record/1460438/>.
 - [3] G. Aad et al. (The ATLAS Collaboration) (2012), 1207.7214.
 - [4] S. Chatrchyan et al. (The CMS Collaboration) (2012), 1207.7235.
 - [5] T. Aaltonen et al. (CDF Collaboration, D0 Collaboration) (2012), 1207.6436.
 - [6] J. Bjorken and S. Weinberg, Phys.Rev.Lett. **38**, 622 (1977).

- [7] B. McWilliams and L.-F. Li, Nucl.Phys. **B179**, 62 (1981).
- [8] O. U. Shanker, Nucl.Phys. **B206**, 253 (1982).
- [9] S. M. Barr and A. Zee, Phys.Rev.Lett. **65**, 21 (1990).
- [10] K. Babu and S. Nandi, Phys.Rev. **D62**, 033002 (2000), hep-ph/9907213.
- [11] J. L. Diaz-Cruz and J. Toscano, Phys.Rev. **D62**, 116005 (2000), hep-ph/9910233.
- [12] T. Han and D. Marfatia, Phys.Rev.Lett. **86**, 1442 (2001), hep-ph/0008141.
- [13] M. Blanke, A. J. Buras, B. Duling, S. Gori, and A. Weiler, JHEP **0903**, 001 (2009), 0809.1073.
- [14] S. Casagrande, F. Goertz, U. Haisch, M. Neubert, and T. Pfoh, JHEP **0810**, 094 (2008), 0807.4937.
- [15] G. F. Giudice and O. Lebedev, Phys.Lett. **B665**, 79 (2008), 0804.1753.
- [16] J. Aguilar-Saavedra, Nucl.Phys. **B821**, 215 (2009), 0904.2387.
- [17] M. E. Albrecht, M. Blanke, A. J. Buras, B. Duling, and K. Gemmler, JHEP **0909**, 064 (2009), 0903.2415.
- [18] A. J. Buras, B. Duling, and S. Gori, JHEP **0909**, 076 (2009), 0905.2318.
- [19] K. Agashe and R. Contino, Phys.Rev. **D80**, 075016 (2009), 0906.1542.
- [20] A. Goudelis, O. Lebedev, and J.-h. Park, Phys.Lett. **B707**, 369 (2012), 1111.1715.
- [21] A. Arhrib, Y. Cheng, and O. C. Kong (2012), 1208.4669.
- [22] D. McKeen, M. Pospelov, and A. Ritz (2012), 1208.4597.
- [23] A. Azatov, M. Toharia, and L. Zhu, Phys.Rev. **D80**, 035016 (2009), 0906.1990.
- [24] G. Blankenburg, J. Ellis, and G. Isidori, Phys.Lett. **B712**, 386 (2012), 1202.5704.
- [25] S. Kanemura, T. Ota, and K. Tsumura, Phys.Rev. **D73**, 016006 (2006), hep-ph/0505191.
- [26] S. Davidson and G. J. Grier, Phys.Rev. **D81**, 095016 (2010), 1001.0434.
- [27] S. Chatrchyan et al. (CMS Collaboration), Phys.Lett. **B713**, 68 (2012), see also <https://twiki.cern.ch/twiki/bin/view/CMSPublic/Hig11029TWiki>, 1202.4083.
- [28] H. Ishimori, T. Kobayashi, H. Ohki, Y. Shimizu, H. Okada, et al., Prog.Theor.Phys.Suppl. **183**, 1 (2010), 1003.3552.
- [29] G. Perez and L. Randall, JHEP **0901**, 077 (2009), 0805.4652.
- [30] J. Lees et al. (BaBar Collaboration) (2012), 1205.5442.
- [31] S. Fajfer, J. F. Kamenik, I. Nisandzic, and J. Zupan (2012), 1206.1872.
- [32] W. Buchmuller and D. Wyler, Nucl.Phys. **B268**, 621 (1986).
- [33] F. del Aguila, M. Perez-Victoria, and J. Santiago, Phys.Lett. **B492**, 98 (2000), hep-

- ph/0007160.
- [34] F. del Aguila, M. Perez-Victoria, and J. Santiago, JHEP **0009**, 011 (2000), hep-ph/0007316.
 - [35] T. Cheng and M. Sher, Phys.Rev. **D35**, 3484 (1987).
 - [36] D. Chang, W. Hou, and W.-Y. Keung, Phys.Rev. **D48**, 217 (1993), hep-ph/9302267.
 - [37] J. Beringer et al. (Particle Data Group), Phys. Rev. **D86**, 010001 (2010).
 - [38] T. Goto, R. Kitano, and S. Mori (2015), 1507.03234.
 - [39] K. Nakamura et al. (Particle Data Group), J. Phys. **G37**, 075021 (2010).
 - [40] U. Bellgardt et al. (SINDRUM Collaboration), Nucl.Phys. **B299**, 1 (1988).
 - [41] K. Hayasaka, K. Inami, Y. Miyazaki, K. Arinstein, V. Aulchenko, et al., Phys.Lett. **B687**, 139 (2010), 1001.3221.
 - [42] L. Willmann, P. Schmidt, H. Wirtz, R. Abela, V. Baranov, et al., Phys.Rev.Lett. **82**, 49 (1999), hep-ex/9807011.
 - [43] T. Clark and S. Love, Mod.Phys.Lett. **A19**, 297 (2004), hep-ph/0307264.
 - [44] G. Bennett et al. (Muon G-2 Collaboration), Phys.Rev. **D73**, 072003 (2006), hep-ex/0602035.
 - [45] The ATLAS collaboration (2012), ATLAS-CONF-2012-094, available from cdsweb.cern.ch/record/1460440/files/ATLAS-CONF-2012-094.pdf.
 - [46] J. Alcaraz et al. (ALEPH Collaboration, DELPHI Collaboration, L3 Collaboration, OPAL Collaboration, LEP Electroweak Working Group) (2006), hep-ex/0612034.
 - [47] S. Dittmaier, S. Dittmaier, C. Mariotti, G. Passarino, R. Tanaka, et al. (2012), 1201.3084.
 - [48] D. Carmi, A. Falkowski, E. Kuflik, T. Volansky, and J. Zupan (2012), 1207.1718.
 - [49] M. Bona et al. (UTfit Collaboration), JHEP **0803**, 049 (2008), 0707.0636.
 - [50] V. M. Abazov et al. (D0 Collaboration), Phys.Lett. **B693**, 81 (2010), 1006.3575.
 - [51] N. Craig, J. A. Evans, R. Gray, M. Park, S. Somalwar, et al. (2012), 1207.6794.
 - [52] M. Gorbahn and U. Haisch (2014), 1404.4873.
 - [53] T. Aaltonen et al. (CDF Collaboration), Phys.Rev.Lett. **102**, 151801 (2009), 0812.3400.
 - [54] G. Aad et al. (ATLAS Collaboration), Phys.Lett. **B712**, 351 (2012), 1203.0529.
 - [55] S. Chatrchyan et al. (CMS Collaboration) (2012), 1208.0957.
 - [56] M. Pospelov and A. Ritz, Annals Phys. **318**, 119 (2005), hep-ph/0504231.
 - [57] G. Aad et al. (ATLAS Collaboration) (2012), 1206.5971.
 - [58] A. Elagin, P. Murat, A. Pranko, and A. Safonov, Nucl.Instrum.Meth. **A654**, 481 (2011), 1012.4686.

- [59] J. Alwall, M. Herquet, F. Maltoni, O. Mattelaer, and T. Stelzer, *JHEP* **1106**, 128 (2011), 1106.0522.
- [60] J. Conway et al., *PGS—Pretty Good Simulation* (2009), <http://physics.ucdavis.edu/conway/research/software/pgs/pgs4-general.htm>.
- [61] S. Davidson, S. Lacroix, and P. Verdier (2012), 1207.4894.
- [62] S. Oryn, X. Rouby, and V. Lemaitre (2009), 0903.2225.
- [63] The CMS collaboration (2011), CMS-PAS-TAU-11-001, available from <http://cdsweb.cern.ch/record/1337004/>.
- [64] J. R. Espinosa, M. Muhlleitner, C. Grojean, and M. Trott (2012), 1205.6790.
- [65] A. Djouadi, A. Falkowski, Y. Mambrini, and J. Quevillon (2012), 1205.3169.
- [66] P. P. Giardino, K. Kannike, M. Raidal, and A. Strumia (2012), 1207.1347.
- [67] R. Kitano, M. Koike, and Y. Okada, *Phys.Rev.* **D66**, 096002 (2002), hep-ph/0203110.
- [68] J. R. Ellis, K. A. Olive, and C. Savage, *Phys.Rev.* **D77**, 065026 (2008), 0801.3656.
- [69] R. D. Young and A. W. Thomas, *Nucl. Phys.* **A844**, 266c (2010), 0911.1757.
- [70] W. H. Bertl et al. (SINDRUM II Collaboration), *Eur.Phys.J.* **C47**, 337 (2006).